

This is a preprint of an article accepted for publication in Journal of Ocean Engineering on 1 May 2015. The published article is available online at <http://www.sciencedirect.com/science/article/pii/S0029801815001699>. To be cited as: Wei K., Bouaanani N., Yuan W. 2015. Simplified methods for efficient seismic design and analysis of water-surrounded composite axisymmetric structures. Journal of Ocean Engineering, 104: 617–638.

Simplified Methods for Efficient Seismic Design and Analysis of Water-Surrounded Composite Axisymmetric Structures

Kai Wei¹, Najib Bouaanani² and Wancheng Yuan³

Abstract: Available simplified formulations for the seismic analysis of axisymmetric structures address materially homogeneous solids with uniform cross-sections, while generally neglecting the effects of higher vibration modes and soil flexibility. In this paper, we develop original simplified procedures that remove these restrictions for practical seismic design and safety evaluation of axisymmetric structures vibrating in contact with water. The procedures proposed take account of higher vibration modes, water compressibility and flexibility of underlying foundation of the structure. For practical purposes, the formulations are first derived while neglecting the effects of surface gravity waves, and are then extended to account for these effects when required. Composite axisymmetric structures made of different materials as well as those with non-uniform hollow cross-sections due to geometric irregularity of interior wall are covered. Step-by-step flowcharts are provided so that calculations can be easily implemented in a daily practical engineering environment. Application of the proposed techniques is illustrated through examples of homogeneous and composite axisymmetric tower-water systems with rigid and flexible foundations. The obtained results are successfully validated against advanced coupled fluid-structure finite element solutions.

Keywords: Axisymmetric structures; Composite structures; Seismic analysis; Fluid-structure interaction; Soil-structure interaction; Vibration periods; Simplified methods.

¹ Graduate Research Assistant, Department of Civil, Geological and Mining Engineering, Polytechnique Montréal, Montréal, QC H3C 3A7, Canada.

² Professor, Department of Civil, Geological and Mining Engineering, Polytechnique Montréal, Montréal, QC H3C 3A7, Canada.
Corresponding author. E-mail: najib.bouaanani@polymtl.ca

³ Professor, State Key Laboratory of Disaster Reduction in Civil Engineering, Tongji University, Shanghai 200092, China.

1 Introduction

Axisymmetric structures surrounded by water are commonly encountered in several civil engineering applications such as offshore platforms, bridge piers, and wind farms. When subjected to earthquake loads, the interaction between an axisymmetric structure and the surrounding water induces hydrodynamic loads while affecting the structural dynamic properties such as natural periods. Earlier literature devoted to the analysis of the vibration characteristics and dynamic response of immersed axisymmetric structures can be roughly classified into three categories depending on the type of modeling adopted for hydrodynamic loads: (i) added-mass formulations where the effect of surrounding water is approximated by added masses distributed along the height of the structure (Lamb 1932, Nagaya and Hai 1985, Chang and Liu 1989, Barltrop and Adams 1991, Spyrakos and Xu 1997, Uściłowska and Kołodziej 1998, Öz 2003, Wu and Chen 2005), (ii) continuum-based solutions where hydrodynamic loads are obtained as analytical solutions of the wave equation governing hydrodynamic pressure (Liaw and Chopra 1974, Eatock Taylor and Duncan 1980, Williams 1986, Tanaka and Hudspeth 1988, Goyal and Chopra 1989, Xing et al. 1997, Wei et al. 2012), and (iii) finite element, boundary element or scaled boundary finite element approaches based on the discretization of the surrounding water (Everstine 1981, Olson and Bathe 1985, Chen 2000, Czygan and Von Estorff 2002, Sigrist and Garreau 2007, Millán et al. 2009, Lu and Jeng 2010, Tao et al. 2007, Meng and Zou 2012, Li et al. 2013, Li et al. 2013, Liu and Lin 2013).

Although the dynamic response of axisymmetric structures surrounded by water can now be solved using coupled fluid-structure finite or boundary elements, most of these techniques have not yet been fully implemented in day-to-day engineering practice, especially at the early stages of seismic design, as they require specialized software or advanced programming, and may result in extensive modeling and computational efforts, combined with high-level expertise. Simplified formulations are therefore still needed to develop efficient procedures that may expedite design and safety evaluation processes. On the other hand, the need for higher structural performance and durability of marine structures suggests increased recourse to composite construction where the efficiencies of various materials can be combined and advantageously optimized. This need is usually coupled to the requirement of using locally available materials for economic or practical reasons. Recent projects illustrate that, in addition to conventional materials such as concrete and steel, researchers and manufacturers are developing new materials such as fiber reinforced polymers that can be used to build composite segments of deep water towers such as wind farms (Gutiérrez et al. 2003, Tricklebank et al. 2007, Seica and Packer 2007, Rashedi et al. 2012, Sun et al. 2012). However, available simplified formulations generally assume that the designed axisymmetric structure has a uniform cross-section and is materially homogeneous, i.e. made with only one material. These methods also usually neglect the effects of higher vibration modes and the flexibility of underlying soil foundation.

In this work, we develop original simplified procedures that waive these restrictive assumptions for enhanced practical seismic design and safety evaluation of axisymmetric structures vibrating in

contact with water. Two types of formulations, i.e. I and II, are proposed depending if the mode shapes of the dry structure, i.e. without water, are obtained using analytical expressions or finite element analysis, respectively. Both proposed formulations take account of higher vibration modes, water compressibility, and flexibility of underlying soil foundation. Formulation type II can also be applied to composite structures made of different materials as well as those with non-uniform hollow cross-sections due to geometric irregularity of the interior wall. The developed methods are assessed through examples that take account of variations in stiffness and mass densities in structures made of several constitutive materials, and having non-uniform hollow cross-sections with irregular interior walls. The effects of higher vibration modes are also included. Expressions are presented considering compressible or incompressible assumptions of surrounding water, as well as rigid or flexible underlying soil foundation. The proposed equations are first derived while neglecting the effects of surface gravity waves and the procedure steps are illustrated in flowcharts in a manner that calculations can be easily implemented in a daily practical engineering environment, for example using simple spreadsheets, as opposed to more sophisticated methods such as coupled fluid-structure finite elements. The formulations are then extended to account for the effects of surface gravity waves when required.

2 Proposed formulations for seismic response of an axisymmetric structure surrounded by water

2.1 Basic assumptions and notations

We consider an axisymmetric structure such as the ones illustrated in Fig. 1. The structure has a total height H_s and is surrounded by an infinite water domain of constant depth H_w . The immersed part of the structure has a uniform outer radius R_s . As illustrated in Fig. 1, two systems of axes are adopted to define the geometry of the system studied: (i) a Cartesian system (x, y, z) , with origin at the center of the bottom cross-section of the structure, and an axis z coinciding with the axis of axisymmetry; and (ii) a cylindrical system (r, θ, z) , where r denotes the radial distance and θ the azimuth between the reference x -axis and the line from the origin to the projection of the point of interest on the (x, y) plane. The response of the structure is studied under the effect of a ground motion acceleration \ddot{u}_g applied along the x direction. The following assumptions are adopted: (i) the axisymmetric structure can be made of one or more materials; (ii) the cross section of the structure can be solid or hollow, and its internal radius may vary as a function of height; (iii) all constitutive materials have a linear elastic behavior during seismic excitation and convective effects in water are neglected; (iv) water is inviscid but can be compressible or incompressible, with its motion irrotational and small in amplitudes; (v) surface gravity waves are neglected. We note that this last assumption is adopted first for practical purposes, it will be waived later in Section 2.5.

2.2 Coupling between hydrodynamic pressure and structural response

The time-history response for radial hydrodynamic pressure exerted at a point of cylindrical coordinates (r, θ, z) is denoted hereafter as $p(r, \theta, z, t)$. It is governed by the classical wave equation

expressed in cylindrical coordinates as (Lamb 1932)

$$\frac{\partial^2 p}{\partial r^2} + \frac{1}{r} \frac{\partial p}{\partial r} + \frac{1}{r^2} \frac{\partial^2 p}{\partial \theta^2} + \frac{\partial^2 p}{\partial z^2} = \frac{1}{C_w^2} \frac{\partial^2 p}{\partial t^2} \quad (1)$$

where C_w is the velocity of sound in water. Hydrodynamic pressure also obeys the following boundary conditions (Liaw and Chopra 1974)

- No surface gravity waves at the free surface $z = H_w$

$$p(r, \theta, H_w, t) = 0 \quad (2)$$

- No vertical motion at the bottom of the surrounding water domain $z = 0$

$$\frac{\partial p}{\partial z}(r, \theta, 0, t) = 0 \quad (3)$$

- Compatibility of displacements and pressure at the water-structure interface $r = R_s$

$$\frac{\partial p}{\partial r}(R_s, \theta, z, t) = -\rho_w \psi_j^{(x)}(z) \cos(\theta) e^{i\omega t} \quad (4)$$

in which ρ_w denotes water density.

- A condition of symmetry about the $x - z$ plane, i.e $\theta = 0$

$$\frac{\partial p}{\partial \theta}(r, 0, z, t) = \frac{\partial p}{\partial \theta}(r, \pi, z, t) \quad (5)$$

Considering a unit harmonic exciting ground acceleration $\ddot{u}_g(t) = e^{i\omega t}$ along the x -axis, with forcing frequency ω , the frequency response function for hydrodynamic pressure can be expressed as $\bar{p}(r, \theta, z, \omega) = p(r, \theta, z, t) e^{-i\omega t}$. The frequency response function for radial hydrodynamic pressure exerted at a point P of coordinates $(r = R_s, \theta = 0, z)$ at the outer surface of the immersed structure including higher vibration mode effects can be decomposed as (Liaw and Chopra 1974, Fenves and Chopra 1984)

$$\bar{p}(R_s, 0, z, \omega) = \bar{p}_0(R_s, 0, z, \omega) - \omega^2 \sum_{j=1}^{N_s} \bar{Z}_j(\omega) \bar{p}_j(R_s, 0, z, \omega) \quad (6)$$

in which \bar{p}_0 is the frequency response function for hydrodynamic pressure due to rigid body motion of the structure, \bar{p}_j is the frequency response function corresponding to hydrodynamic pressure due to horizontal acceleration $\psi_j(z)$ of the structure, where ψ_j denotes the j th structural mode shape along x -direction including the effect of a massless soil foundation when considered in the analysis, \bar{Z}_j is the corresponding generalized coordinate and N_s is the total number of structural mode shapes along the x -direction which are included in the analysis. The time- and frequency-domain responses of radial hydrodynamic pressure at a point of coordinates $(r = R_s, \theta, z)$ of the outer surface of the immersed structure can be obtained from radial hydrodynamic pressure at point P using the following transformations as

$$p(R_s, \theta, z, t) = p(R_s, 0, z, t) \cos(\theta); \quad \bar{p}(R_s, \theta, z, \omega) = \bar{p}(R_s, 0, z, \omega) \cos(\theta) \quad (7)$$

Analytical solutions for hydrodynamic pressure frequency response functions \bar{p}_0 and \bar{p}_j were proposed by Liaw and Chopra (1974) and are briefly reviewed and updated according to this paper's notation in Appendix A.

Using modal superposition and mode shapes orthogonality, we show that the vector of frequency dependent generalized coordinates \bar{Z}_j , $j = 1 \dots N_s$, can be obtained by solving the system of equations

$$\bar{\mathbf{S}} \bar{\mathbf{Z}} = \bar{\mathbf{Q}} \quad (8)$$

in which, for $j = 1 \dots N_s$ and $m = 1 \dots N_s$

$$\bar{S}_{j,m}(\omega) = \left(-\omega^2 + \omega_j^2 + 2i\omega\omega_j\xi_j \right) M_j \delta_{m,j} - \omega^2 B_{j,m}(\omega) \quad (9)$$

$$\bar{Q}_m(\omega) = -L_m - B_{0,m}(\omega) \quad (10)$$

where

$$B_{0,m}(\omega) = R_s \int_0^{H_w} \int_0^{2\pi} \bar{p}_0(R_s, \theta, z, \omega) \cos(\theta) \psi_m(z) d\theta dz \quad (11)$$

$$B_{j,m}(\omega) = R_s \int_0^{H_w} \int_0^{2\pi} \bar{p}_j(R_s, \theta, z, \omega) \cos(\theta) \psi_m(z) d\theta dz \quad (12)$$

and $\delta_{m,j}$ denotes the Kronecker symbol, ω_j the vibration frequency along the j th mode of vibration ψ_j of the dry axisymmetric structure, ξ_j the corresponding modal damping, and M_j and L_m are the associated generalized mass and force given by

$$M_j = \int_0^{H_s} \mu_s(z) [\psi_j(z)]^2 dz; \quad L_m = \int_0^{H_s} \mu_s(z) \psi_m(z) dz \quad (13)$$

where μ_s is the line density of the axisymmetric structure along height. When mode shapes are mass-normalized, the generalized masses have unit values $M_j = 1$, $j = 1 \dots N_s$.

Substituting Eqs. (A1) and (A2) of Appendix A into Eqs. (11) and (12), respectively, and considering Eq. (A4), we obtain for $j = 1 \dots N_s$ and $m = 1 \dots N_s$

$$B_{0,m}(\omega) = \frac{4\pi\rho_w R_s}{H_w} \left[-\sum_{n=1}^{\bar{n}-1} I_{0n} I_{mn} \frac{\mathcal{D}_n(\kappa_n R_s)}{\kappa_n} e^{i\tau_n R_s} + \sum_{n=\bar{n}}^{N_w} I_{0n} I_{mn} \frac{\mathcal{E}_n(\kappa'_n R_s)}{\kappa'_n} \right] \quad (14)$$

$$B_{j,m}(\omega) = \frac{4\pi\rho_w R_s}{H_w} \left[-\sum_{n=1}^{\bar{n}-1} I_{jn} I_{mn} \frac{\mathcal{D}_n(\kappa_n R_s)}{\kappa_n} e^{i\tau_n R_s} + \sum_{n=\bar{n}}^{N_w} I_{jn} I_{mn} \frac{\mathcal{E}_n(\kappa'_n R_s)}{\kappa'_n} \right] \quad (15)$$

where N_w is the number of considered acoustical water modes, and the parameters \bar{n} , λ_n , κ_n , κ'_n , I_{0n} , I_{jn} , \mathcal{D}_n , \mathcal{E}_n and τ_n are given in Appendix A. The following practical expressions of the last three parameters are proposed in this work to further simplify and expedite the computation of the

parameters $B_{0,m}$ and $B_{j,m}$ for $j = 1 \dots N_s$ and $m = 1 \dots N_s$

$$\mathcal{D}_n(\kappa_n R_s) = \frac{0.5 (\kappa_n R_s)^3 - 0.038 (\kappa_n R_s)^2 + 0.249 \kappa_n R_s}{(\kappa_n R_s)^3 - 0.013 (\kappa_n R_s)^2 + 0.019 \kappa_n R_s + 0.473} \quad (16)$$

$$\mathcal{E}_n(\kappa'_n R_s) = \frac{0.5 (\kappa'_n R_s)^2 + 0.345 \kappa'_n R_s}{(\kappa'_n R_s)^2 + 1.202 (\kappa'_n R_s) + 0.670} \quad (17)$$

$$\tau_n R_s = \tan^{-1} \left[\frac{-3.06 (\kappa_n R_s)^2 + 0.14 \kappa_n R_s - 0.006}{\kappa_n R_s + 1.46} \right] \quad (18)$$

The accuracy of these approximations is illustrated in Fig. 2 which compares the results of Eqs. (16) to (18) to those of the exact expressions Eqs. (A5) to (A7), respectively.

We note that the effects of water compressibility have been studied previously by several researchers such as Liaw and Chopra (1974) and Tanaka and Hudspeth (1988). These studies showed that the effects of water compressibility on dynamic structural response should generally be included for flexible water-surrounded structures with low slenderness ratios R_s/H_w of about 0.25 or less. It was namely found that water compressibility reduces response amplitudes at higher modes of vibration of such squat structures mainly because of added damping. If water is assumed incompressible, the parameters $B_{0,m}$ and $B_{j,m}$ become frequency-independent as Eqs. (14) and (15) simplify to

$$B_{0,m} = \frac{4\pi \rho_w R_s}{H_w} \left[\sum_{n=1}^{N_w} I_{0n} I_{mn} \frac{\mathcal{E}_n(\kappa'_n R_s)}{\kappa'_n} \right] \quad (19)$$

$$B_{j,m} = \frac{4\pi \rho_w R_s}{H_w} \left[\sum_{n=1}^{N_w} I_{jn} I_{mn} \frac{\mathcal{E}_n(\kappa'_n R_s)}{\kappa'_n} \right] \quad (20)$$

To solve the system of Eqs. (8), the frequencies and mode shapes of the dry axisymmetric structure are to be determined first. For this purpose, two procedures based on an analytical formulation of mode shapes and a finite element solution, respectively, are proposed hereafter.

2.3 Solution based on analytical formulation of mode shapes

The analytical formulation described here applies only to cylindrical cantilever structures with a uniform cross-section. Assuming an Euler-Bernoulli beam behavior, the mode shape ψ_j , $j = 1 \dots N_s$, of the dry structure can be expressed as (Clough and Penzien 1993)

$$\psi_j(z) = A_1^{(j)} \cos(\beta_j z) + A_2^{(j)} \sin(\beta_j z) + A_3^{(j)} \cosh(\beta_j z) + A_4^{(j)} \sinh(\beta_j z) \quad (21)$$

where β_j is an eigenvalue related to the j th frequency ω_j of the dry structure by

$$\beta_j^4 = \frac{\omega_j^2 \mu_s}{E_s I_s}; \quad \omega_j = \beta_j^2 \sqrt{\frac{E_s I_s}{\mu_s}} \quad (22)$$

and $A_1^{(j)}$, $A_2^{(j)}$, $A_3^{(j)}$ and $A_4^{(j)}$ are unknown real constants to be determined using the following four boundary conditions (Michaltsos and Ermopoulos 2001, Wu and Chen 2005)

$$E_s I_s \psi'''(0) = -K_T \psi(0) \quad (23)$$

$$E_s I_s \psi''(0) = K_R \psi'(0) \quad (24)$$

$$E_s I_s \psi''(H_s) = m_0 e \omega^2 \psi(H_s) + (J_0 + m_0 e^2) \omega^2 \psi'(H_s) \quad (25)$$

$$E_s I_s \psi'''(H_s) = -m_0 \omega^2 \psi(H_s) - m_0 e \omega^2 \psi'(H_s) \quad (26)$$

in which $E_s I_s$ is the flexural rigidity, m_0 is the rigid tip mass lumped at a distance e of the top of the structure, J_0 is the corresponding rotary moment of inertia, and K_T and K_R are the translational and rotational stiffness coefficients at the base of the structure, respectively.

Substituting Eq. (21) into Eqs. (23) to (26), we obtain a system of equations (Auciello 1996)

$$\begin{bmatrix} \alpha_{11}^{(j)} & \alpha_{12}^{(j)} & \alpha_{13}^{(j)} & \alpha_{14}^{(j)} \\ \alpha_{21}^{(j)} & \alpha_{22}^{(j)} & \alpha_{23}^{(j)} & \alpha_{24}^{(j)} \\ \alpha_{31}^{(j)} & \alpha_{32}^{(j)} & \alpha_{33}^{(j)} & \alpha_{34}^{(j)} \\ \alpha_{41}^{(j)} & \alpha_{42}^{(j)} & \alpha_{43}^{(j)} & \alpha_{44}^{(j)} \end{bmatrix} \begin{bmatrix} A_1^{(j)} \\ A_2^{(j)} \\ A_3^{(j)} \\ A_4^{(j)} \end{bmatrix} = 0 \quad (27)$$

in which

$$\alpha_{11}^{(j)} = \alpha_{13}^{(j)} = K_T; \quad \alpha_{12}^{(j)} = -\alpha_{14}^{(j)} = -E_s I_s \beta_j^3 \quad (28)$$

$$\alpha_{21}^{(j)} = -\alpha_{23}^{(j)} = -E_s I_s \beta_j^2; \quad \alpha_{22}^{(j)} = \alpha_{24}^{(j)} = -K_R \beta_j \quad (29)$$

$$\alpha_{31}^{(j)} = \frac{\beta_j^5 (m_0 e^2 + J_0) \sin(\beta_j H_s)}{\mu_s} - \beta_j^2 \cos(\beta_j H_s) - \frac{\beta_j^4 m_0 e \cos(\beta_j H_s)}{\mu_s} \quad (30)$$

$$\alpha_{32}^{(j)} = -\beta_j^2 \sin(\beta_j H_s) - \frac{\beta_j^5 (m_0 e^2 + J_0) \cos(\beta_j H_s)}{\mu_s} - \frac{\beta_j^4 m_0 e \sin(\beta_j H_s)}{\mu_s} \quad (31)$$

$$\alpha_{33}^{(j)} = \beta_j^2 \cosh(\beta_j H_s) - \frac{\beta_j^5 (m_0 e^2 + J_0) \sinh(\beta_j H_s)}{\mu_s} - \frac{\beta_j^4 m_0 e \cosh(\beta_j H_s)}{\mu_s} \quad (32)$$

$$\alpha_{34}^{(j)} = \beta_j^2 \sinh(\beta_j H_s) - \frac{\beta_j^5 (m_0 e^2 + J_0) \cosh(\beta_j H_s)}{\mu_s} - \frac{\beta_j^4 m_0 e \sinh(\beta_j H_s)}{\mu_s} \quad (33)$$

$$\alpha_{41}^{(j)} = \beta_j^3 \sin(\beta_j H_s) + \frac{\beta_j^4 m_0 \cos(\beta_j H_s)}{\mu_s} - \frac{\beta_j^5 m_0 e \sin(\beta_j H_s)}{\mu_s} \quad (34)$$

$$\alpha_{42}^{(j)} = -\beta_j^3 \cos(\beta_j H_s) + \frac{\beta_j^4 m_0 \sin(\beta_j H_s)}{\mu_s} + \frac{\beta_j^5 m_0 e \cos(\beta_j H_s)}{\mu_s} \quad (35)$$

$$\alpha_{43}^{(j)} = \beta_j^3 \sinh(\beta_j H_s) + \frac{\beta_j^4 m_0 \cosh(\beta_j H_s)}{\mu_s} + \frac{\beta_j^5 m_0 e \sinh(\beta_j H_s)}{\mu_s} \quad (36)$$

$$\alpha_{44}^{(j)} = \beta_j^3 \cosh(\beta_j H_s) + \frac{\beta_j^4 m_0 \sinh(\beta_j H_s)}{\mu_s} + \frac{\beta_j^5 m_0 e \cosh(\beta_j H_s)}{\mu_s} \quad (37)$$

The system of equations (27) admits a non trivial solution if and only if

$$\det \begin{bmatrix} \alpha_{11}^{(j)} & \alpha_{12}^{(j)} & \alpha_{13}^{(j)} & \alpha_{14}^{(j)} \\ \alpha_{21}^{(j)} & \alpha_{22}^{(j)} & \alpha_{23}^{(j)} & \alpha_{24}^{(j)} \\ \alpha_{31}^{(j)} & \alpha_{32}^{(j)} & \alpha_{33}^{(j)} & \alpha_{34}^{(j)} \\ \alpha_{41}^{(j)} & \alpha_{42}^{(j)} & \alpha_{43}^{(j)} & \alpha_{44}^{(j)} \end{bmatrix} = 0 \quad (38)$$

Expansion of Eq. (38) leads to a transcendental equation which has an infinite number of roots. It can be solved for frequency coefficients $\beta_1, \beta_2, \dots, \beta_j, \dots$ using *Regula falsi* method (Mathews 1992, MATLAB 2011). Using $A_1^{(j)}$ as a normalization factor of the shape functions, the relationship between the ratios $A_2^{(j)}/A_1^{(j)}$, $A_3^{(j)}/A_1^{(j)}$ and $A_4^{(j)}/A_1^{(j)}$ can be obtained by solving the system of equations

$$\begin{bmatrix} \alpha_{12}^{(j)} & \alpha_{13}^{(j)} & \alpha_{14}^{(j)} \\ \alpha_{22}^{(j)} & \alpha_{23}^{(j)} & \alpha_{24}^{(j)} \\ \alpha_{32}^{(j)} & \alpha_{33}^{(j)} & \alpha_{34}^{(j)} \end{bmatrix} \begin{bmatrix} \frac{A_2^{(j)}}{A_1^{(j)}} \\ \frac{A_3^{(j)}}{A_1^{(j)}} \\ \frac{A_4^{(j)}}{A_1^{(j)}} \end{bmatrix} = \begin{bmatrix} -\alpha_{11}^{(j)} \\ -\alpha_{21}^{(j)} \\ -\alpha_{31}^{(j)} \end{bmatrix} \quad (39)$$

The mode shapes ψ_j can then be determined by introducing the values of β_j , $A_1^{(j)}$, $A_2^{(j)}$, $A_3^{(j)}$ and $A_4^{(j)}$ into Eq. (21). Introducing Eq. (21) into the expression of the integral I_{jn} given in Eq. (A4) yields

$$I_{jn} = A_1^{(j)} \left(\chi_{jn}^{(1)} + \frac{A_2^{(j)}}{A_1^{(j)}} \chi_{jn}^{(2)} + \frac{A_3^{(j)}}{A_1^{(j)}} \chi_{jn}^{(3)} + \frac{A_4^{(j)}}{A_1^{(j)}} \chi_{jn}^{(4)} \right) \quad (40)$$

where

$$\chi_{jn}^{(1)} = \int_0^{H_w} \cos(\lambda_n z) \cos(\beta_j z) dz = \frac{\lambda_n \cos(\beta_j H_w) \sin(\lambda_n H_w)}{\lambda_n^2 - \beta_j^2} \quad (41)$$

$$\chi_{jn}^{(2)} = \int_0^{H_w} \cos(\lambda_n z) \sin(\beta_j z) dz = \frac{\lambda_n \sin(\beta_j H_w) \sin(\lambda_n H_w) - \beta_j}{\lambda_n^2 - \beta_j^2} \quad (42)$$

$$\chi_{jn}^{(3)} = \int_0^{H_w} \cos(\lambda_n z) \cosh(\beta_j z) dz = \frac{\lambda_n \cosh(\beta_j H_w) \sin(\lambda_n H_w)}{\lambda_n^2 + \beta_j^2} \quad (43)$$

$$\chi_{jn}^{(4)} = \int_0^{H_w} \cos(\lambda_n z) \sinh(\beta_j z) dz = \frac{\lambda_n \sinh(\beta_j H_w) \sin(\lambda_n H_w) - \beta_j}{\lambda_n^2 + \beta_j^2} \quad (44)$$

2.4 Solution based on finite element determination of mode shapes

The analytical formulation described in the previous section assumes that the structure studied is a cylindrical cantilever with a uniform cross-section. More general axisymmetric structures such as the one illustrated in Fig. 1 (c) require recourse to 3D finite element modeling since they can be made of one or more materials and have non-uniform hollow cross-sections. Such finite element analysis can be conducted using standard finite element software that includes only classical solid finite elements and not necessarily fluid-structure interaction capabilities. The obtained lateral structural mode shapes ψ_j along the axis of axisymmetry of the studied structure, can be approximated by a polynomial function of order N_{ψ_j} , $j = 1 \dots N_s$

$$\psi_j(z) \approx \sum_{k=0}^{N_{\psi_j}} a_{j,k} \left(\frac{z}{H_s} \right)^k \quad (45)$$

in which the coefficients $a_{j,k}$ can be determined using a classical fitting technique. The term $a_{j,0} = \psi_j(0)$ takes account of translations due to soil flexibility as illustrated in Fig. 3.

It is important to note that 3D finite element modal analysis of an axisymmetric structure yields pairs of lateral mode shapes along two orthogonal directions. Each pair corresponds to one natural frequency. In the present work, the number N_s of mode shapes includes only those modes which are along the x -direction corresponding to that of the applied ground motion \ddot{u}_g . We also note that the values of the mode shapes can be taken along the axis of axisymmetry or along the line of intersection of plane xz and the structure as indicated in Fig. 3.

On substituting Eq. (45) into the integral given by Eq. (A4) of Appendix A, we obtain

$$I_{jn} = \sum_{k=0}^{N_{\psi_j}} \frac{a_{j,k}}{H_s^k} \int_0^{H_w} \cos(\lambda_n z) z^k dz \quad (46)$$

Bouaanani and Perrault (2010) (Bouaanani and Perrault 2010) showed that I_{jn} can also be expressed as

$$I_{jn} = F_{jn} I_{0n} + G_{jn} \quad (47)$$

where

$$F_{jn} = \sum_k \left\{ \left[\sum_{\ell=0}^k (-1)^{k-\ell} \frac{\Lambda_{2\ell}(\lambda_n H_w)}{\Lambda_{2k}(\lambda_n H_s)} \right] a_{j,2k} + \left[\sum_{\ell=0}^k (-1)^{k-\ell} \frac{\Lambda_{2\ell+1}(\lambda_n H_w)}{\Lambda_{2k+1}(\lambda_n H_s)} \right] a_{j,2k+1} \right\} \quad (48)$$

$$G_{jn} = -\frac{1}{\lambda_n H_w} \sum_k \left\{ \left[\frac{(-1)^k}{\Lambda_{2k+1}(\lambda_n H_s)} \right] a_{j,2k+1} \right\} \quad (49)$$

with the function Λ_m defined as

$$\Lambda_m(z) = \frac{z^m}{m!} \quad (50)$$

where z and m are real and integer numbers, respectively. Substituting Eq. (47) into Eqs. (14) and (15) respectively, yields the following expressions for parameters $B_{0,m}$ and $B_{j,m}$ for $j = 1 \dots N_s$ and $m = 1 \dots N_s$

$$B_{0,m} = \frac{4\pi\rho_w R_s}{H_w} \left\{ -\sum_{n=1}^{\bar{n}-1} \frac{[F_{mn} + (-1)^{n+1} \lambda_n G_{mn}] \mathcal{D}_n(\kappa_n R_s)}{\lambda_n^2 \kappa_n} e^{i\tau_n R_s} + \sum_{n=\bar{n}}^{N_w} \frac{[F_{mn} + (-1)^{n+1} \lambda_n G_{mn}] \mathcal{E}_n(\kappa'_n R_s)}{\lambda_n^2 \kappa'_n} \right\} \quad (51)$$

$$B_{j,m} = \frac{4\pi\rho_w R_s}{H_w} \left\{ -\sum_{n=1}^{\bar{n}-1} \frac{F_{jn} [F_{mn} + (-1)^{n+1} \lambda_n G_{mn}] \mathcal{D}_n(\kappa_n R_s)}{\lambda_n^2 \kappa_n} e^{i\tau_n R_s} - \sum_{n=1}^{\bar{n}-1} \frac{\lambda_n G_{jn} [(-1)^{n+1} F_{mn} + \lambda_n G_{mn}] \mathcal{D}_n(\kappa_n R_s)}{\lambda_n^2 \kappa_n} e^{i\tau_n R_s} + \sum_{n=\bar{n}}^{N_w} \frac{F_{jn} [F_{mn} + (-1)^{n+1} \lambda_n G_{mn}] \mathcal{E}_n(\kappa'_n R_s)}{\lambda_n^2 \kappa'_n} + \sum_{n=\bar{n}}^{N_w} \frac{\lambda_n G_{jn} [(-1)^{n+1} F_{mn} + \lambda_n G_{mn}] \mathcal{E}_n(\kappa'_n R_s)}{\lambda_n^2 \kappa'_n} \right\} \quad (52)$$

where the parameters λ_n , κ_n , κ'_n , \mathcal{D}_n , \mathcal{E}_n and τ_n are given by Eqs. (A3) and (A5) to (A7) of Appendix A.

When water compressibility is neglected, Eqs. (51) and (52) simplify to

$$B_{0,m} = \frac{4\pi\rho_w R_s}{H_w} \left\{ \sum_{n=1}^{N_w} \frac{[F_{mn} + (-1)^{n+1} \lambda_n G_{mn}] \mathcal{E}_n(\kappa'_n R_s)}{\lambda_n^2 \kappa'_n} \right\} \quad (53)$$

$$B_{j,m} = \frac{4\pi\rho_w R_s}{H_w} \left\{ \sum_{n=1}^{N_w} \frac{F_{jn} [F_{mn} + (-1)^{n+1} \lambda_n G_{mn}] \mathcal{E}_n(\kappa'_n R_s)}{\lambda_n^2 \kappa'_n} \right. \\ \left. + \sum_{n=1}^{N_w} \frac{\lambda_n G_{jn} [(-1)^{n+1} F_{mn} + \lambda_n G_{mn}] \mathcal{E}_n(\kappa'_n R_s)}{\lambda_n^2 \kappa'_n} \right\} \quad (54)$$

in which all the parameters are given by the same equations as previously, except κ'_n which is obtained from Eq. (A12) of Appendix A.

2.5 Effects of surface gravity waves

The effects of surface gravity waves on the seismic response of water-surrounded structures are known to be generally small and limited to the low frequency range (Liaw and Chopra 1974; Goyal and Chopra 1989). For comprehensiveness however, we provide the following equations to account for the effects of surface gravity waves when required. In this case, the boundary condition in Eq. (2) of the manuscript has to be changed to

$$\frac{\partial^2 p}{\partial t^2}(r, \theta, H_w, t) = -g \frac{\partial p}{\partial z}(r, \theta, H_w, t) \quad (55)$$

where g denotes gravity acceleration. Considering this new boundary condition and solving the wave equation (1) for hydrodynamic pressure frequency response functions \bar{p}_0 and \bar{p}_j , $j = 1 \dots N_s$, Liaw and Chopra (1974) showed that Eqs. (A1) and (A2) of Appendix A have to be replaced by Eqs. (A13) and (A14) of the same appendix, respectively. The following remarks can then be made to evaluate the main additional calculations involved when surface gravity waves are to be included in the analysis:

- Contrary to obtaining the values of eigenvalue λ_n through the closed-form expressions in Eq. (A3), these parameters can be determined only numerically by solving Eq. (A16) when surface gravity waves are included.
- Additional parameters λ_0 and κ_0 have to be determined numerically by solving Eq. (A15).
- The first sums in each of Eqs. (A13) and (A14) have to be determined to obtain hydrodynamic pressures \bar{p}_0 and \bar{p}_j , $j = 1 \dots N_s$.

Substituting Eqs. (A13) and (A14) into Eqs. (11) and (12), respectively, we obtain new expressions

for the quantities $B_{0,m}$ and $B_{j,m}$, $j=1 \dots N_s$, $m=1 \dots N_s$, and Eqs. (14) and (14) transform to

$$B_{0,m}(\omega) = 8\pi\rho_w R_s \left\{ -\frac{\lambda_0 I_{00} I_{m0} \mathcal{D}_0(\kappa_0 R_s)}{\kappa_0 [2\lambda_0 H_w + \sinh(2\lambda_0 H_w)]} e^{i\tau_0 R_s} - \sum_{n=1}^{\bar{n}-1} \frac{\lambda_n I_{0n} I_{mn} \mathcal{D}_n(\kappa_n R_s)}{\kappa_n [2\lambda_n H_w + \sin(2\lambda_n H_w)]} e^{i\tau_n R_s} + \sum_{n=\bar{n}}^{N_w} \frac{\lambda_n I_{0n} I_{mn} \mathcal{E}_n(\kappa'_n R_s)}{\kappa'_n [2\lambda_n H_w + \sin(2\lambda_n H_w)]} \right\} \quad (56)$$

$$B_{j,m}(\omega) = 8\pi\rho_w R_s \left\{ -\frac{\lambda_0 I_{j0} I_{m0} \mathcal{D}_0(\kappa_0 R_s)}{\kappa_0 [2\lambda_0 H_w + \sinh(2\lambda_0 H_w)]} e^{i\tau_0 R_s} - \sum_{n=1}^{\bar{n}-1} \frac{\lambda_n I_{jn} I_{mn} \mathcal{D}_n(\kappa_n R_s)}{\kappa_n [2\lambda_n H_w + \sin(2\lambda_n H_w)]} e^{i\tau_n R_s} + \sum_{n=\bar{n}}^{N_w} \frac{\lambda_n I_{jn} I_{mn} \mathcal{E}_n(\kappa'_n R_s)}{\kappa'_n [2\lambda_n H_w + \sin(2\lambda_n H_w)]} \right\} \quad (57)$$

where N_w is the number of considered acoustical water modes and the parameters κ'_n , I_{jn} , \mathcal{D}_n , \mathcal{E}_n and τ_n are given by the same equations as previously, while λ_0 and λ_n are numerical solutions of Eqs. (A15) and (A16) of Appendix A and κ_0 , κ_n , I_{00} , I_{0n} , and I_{j0} are given by Eqs. (A17) to . As previously, the integer \bar{n} in the second sums of Eqs. (58) and (59) denotes the smallest value of integer n such that $\lambda_n > \frac{\omega}{C_w}$. Following the same approach described previously, new simplified expressions for parameters $B_{0,m}$ and $B_{j,m}$, $j=1 \dots N_s$, $m=1 \dots N_s$, are proposed

$$B_{0,m}(\omega) = 8\pi\rho_w R_s \left\{ -\frac{\lambda_0 I_{00} [I_{00} F_{m0}(i\lambda_0) + G_{m0}(i\lambda_0)] \mathcal{D}_0(\kappa_0 R_s)}{\kappa_0 [2\lambda_0 H_w + \sinh(2\lambda_0 H_w)]} e^{i\tau_0 R_s} - \sum_{n=1}^{\bar{n}-1} \frac{\lambda_n I_{0n} [I_{0n} F_{mn}(\lambda_n) + G_{mn}(\lambda_n)] \mathcal{D}_n(\kappa_n R_s)}{\kappa_n [2\lambda_n H_w + \sin(2\lambda_n H_w)]} e^{i\tau_n R_s} + \sum_{n=\bar{n}}^{N_w} \frac{\lambda_n I_{0n} [I_{0n} F_{mn}(\lambda_n) + G_{mn}(\lambda_n)] \mathcal{E}_n(\kappa'_n R_s)}{\kappa'_n [2\lambda_n H_w + \sin(2\lambda_n H_w)]} \right\} \quad (58)$$

$$\begin{aligned}
B_{j,m}(\omega) = 8\pi\rho_w R_s \left\{ \right. & - \frac{\lambda_0 [I_{00} F_{j0}(i\lambda_0) + G_{j0}(i\lambda_0)] [I_{00} F_{m0}(i\lambda_0) + G_{m0}(i\lambda_0)] \mathcal{D}_0(\kappa_0 R_s)}{\kappa_0 [2\lambda_0 H_w + \sinh(2\lambda_0 H_w)]} e^{i\tau_0 R_s} \\
& - \sum_{n=1}^{\bar{n}-1} \frac{\lambda_n [I_{0n} F_{jn}(\lambda_n) + G_{jn}(\lambda_n)] [I_{0n} F_{mn}(\lambda_n) + G_{mn}(\lambda_n)] \mathcal{D}_n(\kappa_n R_s)}{\kappa_n [2\lambda_n H_w + \sin(2\lambda_n H_w)]} e^{i\tau_n R_s} \\
& \left. + \sum_{n=\bar{n}}^{N_w} \frac{\lambda_n [I_{0n} F_{mn}(\lambda_n) + G_{mn}(\lambda_n)] \mathcal{E}_n(\kappa'_n R_s)}{\kappa'_n [2\lambda_n H_w + \sin(2\lambda_n H_w)]} \right\}
\end{aligned} \tag{59}$$

It can be seen from Eqs. (55), (A13) and (A14) that the effects of surface gravity waves are concentrated in the very low frequency range and that they vanish rapidly as frequencies increase. In the limiting case $\omega \rightarrow +\infty$, we can easily show that including or neglecting the effects of surface gravity waves yield the same results, since: (i) the solutions of Eq. (55) are the same as those given by Eq. (A3) when surface gravity waves are neglected, and (ii) the first sums in Eqs. (A13) and (A14) vanish. Therefore, surface gravity waves could affect structural seismic response only if: (i) the vibration frequencies of the water-surrounded structure are very low, and (ii) the earthquake ground motion is rich of low frequency content in the same range as the structure.

2.6 Hydrodynamic pressure and structural response due to seismic loading

The vector $\bar{\mathbf{Z}}$ of complex-valued frequency response functions is first determined from Eq. (8) for frequencies in the range of interest. Eq. (6) is then applied to obtain frequency response functions for hydrodynamic pressure, and those for structural lateral displacements and accelerations can be expressed as

$$\bar{u}(z, \omega) = \sum_{j=1}^{N_s} \psi_j(z) \bar{Z}_j(\omega); \quad \bar{\ddot{u}}(z, \omega) = -\omega^2 \sum_{j=1}^{N_s} \psi_j(z) \bar{Z}_j(\omega) \tag{60}$$

where \bar{u} and $\bar{\ddot{u}}$ denote the lateral displacement and acceleration along ground motion direction x , respectively.

The time-history response of the real part of hydrodynamic pressure along the direction x of application of ground acceleration $\ddot{u}_g(t)$ can be obtained as

$$\text{Re} [p(R_s, \theta, z, t)] = \frac{1}{2\pi} \int_{-\infty}^{\infty} \bar{p}^*(R_s, \theta, z, \omega) \bar{\ddot{u}}_g(\omega) e^{i\omega t} d\omega \tag{61}$$

where \bar{p}^* denotes the complex conjugate of hydrodynamic pressure frequency response function \bar{p} given by Eq.(6).

The structural displacement and acceleration time-history response to a ground acceleration $\ddot{u}_g(t)$

applied along the x direction can be obtained as

$$u(z, t) = \sum_{j=1}^{N_s} \psi_j(z) Z_j(t); \quad \ddot{u}(z, t) = \sum_{j=1}^{N_s} \psi_j(z) \ddot{Z}_j(t) \quad (62)$$

where the time-domain generalized coordinates $Z_j(t)$ are given by the Fourier integrals

$$Z_j(t) = \frac{1}{2\pi} \int_{-\infty}^{\infty} \bar{Z}_j(\omega) \bar{\ddot{u}}_g(\omega) e^{i\omega t} d\omega; \quad \ddot{Z}_j(t) = -\frac{1}{2\pi} \int_{-\infty}^{\infty} \omega^2 \bar{Z}_j(\omega) \bar{\ddot{u}}_g(\omega) e^{i\omega t} d\omega \quad (63)$$

in which $\bar{\ddot{u}}_g(\omega)$ is the Fourier transform of the ground acceleration $\ddot{u}_g(t)$

$$\bar{\ddot{u}}_g(\omega) = \int_0^{t_a} \ddot{u}_g(t) e^{-i\omega t} dt \quad (64)$$

in which t_a is the time duration of the applied accelerogram.

3 Illustrative examples

The dynamic responses of simple and complex axisymmetric structures are investigated in this section to verify and illustrate the applicability of the proposed methods. The description as well as the frequency- and time-domain analyses of the studied systems are presented next.

The developed formulations were programmed using MATLAB (MATLAB 2011) according to the flowcharts in Fig. 4 and 5. The flowchart in Fig. 4 shows the proposed procedure to determine the dynamic response based on the analytical formulation of the mode shapes of the studied axisymmetric structure as presented in Section 2.3. This method is referred to as analysis type I hereafter. Fig. 5 illustrates the flowchart to be applied when finite element determination of mode shapes and their interpolation are used instead of the analytical formulation as described in Section 2.4. This method is referred to as analysis type II hereafter. For clarity, both flowcharts in Figs. 4 and 5 refer to equation numbers from the previous sections. We also note that for brevity, the flowcharts are presented only for the most common cases where effects surface gravity waves can be neglected. The flowcharts can be adapted easily considering the equations given in Section 2.5.

In this section, we assess the effectiveness of these formulations in determining the seismic response of 3D axisymmetric towers surrounded by water. Four examples are proposed next to illustrate the application of the proposed methods and assess their ability to account for various parameters including composite construction, non-uniform structure's cross-section, higher vibration modes, soil flexibility and surface gravity waves.

3.1 Example 1: Seismic response of a tower with a uniform solid cross-section

In this example, we investigate the dynamic response of a 42 m high axisymmetric cylindrical tower illustrated in Fig. 6(a). The tower has a 4 m diameter uniform solid cross-section and is surrounded by an infinite water domain as indicated in Fig. 6(b). It is made of a material with an elastic modulus $E_s = 25$ GPa, a mass density $\rho_s = 2500$ kg/m³ and a Poisson's ratio $\nu = 0.2$.

Water is considered compressible, with a velocity of pressure waves $C_w = 1440$ m/s and a mass density $\rho_w = 1000$ kg/m³. Both cases of rigid and flexible soil foundations underlying the tower are considered while the effects of surface gravity waves are neglected.

The seismic analysis of the cylindrical tower subjected to the horizontal N-S component of the 1940 Imperial Valley earthquake recorded on rock site at El Centro (PEER 2011) is conducted using analysis types I and II. Fig. 7 shows the corresponding accelerogram and displacement time-history nondimensionalized by the peak ground acceleration (PGA) $|\ddot{u}_g|_{\max} = 0.313$ g and peak ground displacement (PGD) $|u_g|_{\max} = 0.133$ m, respectively. The ground motion is applied along the x -direction and computations are conducted neglecting soil flexibility at first. A constant modal damping ratio $\xi = 5\%$ is assigned to all the modes included in the analysis. Fig. 8 (a) illustrates the first four modes of vibration ψ_j , $j = 1 \dots 4$, and corresponding vibration frequencies of the cylindrical structure obtained and used in analysis type I. Analysis type II is also conducted for comparison purposes. In this case, the software ADINA (2014) is used to discretize the tower into 20-node solid 3D finite elements according to the mesh density illustrated in Fig. 9 (a). The resulting four mode shapes included in the analysis are shown in Fig. 8 (b).

A coupled 3D finite element analysis of the tower-water system is carried out to validate the results of analysis types I and II. The tower and surrounding water are then modeled using 3D 20-node solid and potential-based finite elements from ADINA as illustrated in Fig. 9 (b). A fixed rigid wall boundary condition is applied at a far end located at a radius of $2H_w = 60$ m around the structure. Fluid-structure interaction is accounted for through special interface elements included in ADINA. The bulk modulus of the potential-based fluid elements is determined as $\rho_w C_w^2 = 2.07$ GPa. The performance of the potential-based formulation and the fluid-structure interface elements was assessed in a previous work (Bouaanani and Lu 2009). The results of the coupled finite element model are denoted as the reference solution in what follows.

The obtained time-histories of hydrodynamic pressure at 6 m above the heel of the tower, i.e. Point A in Fig. 9, and horizontal acceleration and displacement along x -direction at the top of the tower, i.e. Point B in Fig. 9, are nondimensionalized with respect to the maximum hydrostatic pressure $\rho_w g H_w$ at the heel of the tower, the PGA and PGD of the applied ground motion, respectively. Fig. 10 compares the results obtained using the coupled finite element model, i.e. reference solution, to those of proposed analysis types I and II. It can be seen that the seismic responses predicted using the proposed methods are in close agreement with the finite element solutions.

Soil flexibility is included next using spring elements introduced between the bottom of the tower and the underlying ground. A stiffness $K_T = 1.0 \times 10^8$ N/m along the horizontal direction and $K_V = 5.0 \times 10^9$ N/m along the vertical direction are adopted for the finite element model without water to calculate the mode shapes for analysis type II. The rotational stiffness K_R required in

analysis type I is related to the vertical stiffness K_V using the following equation

$$K_R = \frac{K_V}{A_s} I_s \quad (65)$$

in which A_s and I_s denote the area and moment of inertia of the bottom cross-section of the tower, respectively. Equivalent distributed soil stiffness is introduced in the coupled finite element model to obtain the reference solution. Fig. 11 shows the mode shapes and corresponding vibration frequencies obtained using the analytical formulation and finite elements including soil flexibility. A very good agreement is observed in Fig. 12 which compares the time-histories of hydrodynamic pressure at Point A and horizontal acceleration and displacement along x -direction at Point B obtained from analysis types I and II to reference solutions. This example shows that both analysis types I and II yield almost identical results for axisymmetric towers with a uniform solid sections laying on whether rigid or flexible soil foundations.

3.2 Example 2: Hollow-section axisymmetric tower with a tip mass

In this example, we investigate the seismic response of a 47 m high axisymmetric tower illustrated in Fig. 13 (a). The 42 m-high lower part of the tower has a hollow cross-section with 4 m and 8 m interior and exterior diameters, respectively. The top of the tower is made of a solid cylindrical part with a diameter of 12 m. The structure is surrounded by an infinite water domain as indicated in Fig. 13 (b). The lower hollow part of the tower is made of a material with an elastic modulus $E_s = 25$ GPa, a mass density $\rho_s = 2500$ kg/m³ and a Poisson's ratio $\nu = 0.2$. The constitutive material of the top part has an elastic modulus $E_s = 30$ GPa, a Poisson's ratio $\nu = 0.2$ and a mass density $\rho_s = 884$ kg/m³ yielding to a total mass of 500 t. Water is assumed compressible, with the same properties as in Example 1. The effects of surface gravity waves are neglected.

The earthquake input is the same as in Example 1. A constant modal damping ratio $\xi = 5\%$ is assigned to all the modes included in the analysis and both rigid and flexible soil assumptions are considered as previously. Fig. 14 shows the finite element model of the tower without water as well as the coupled 3D finite element model of the tower-water system constructed to obtain the reference solution. Four mode shapes and corresponding vibration frequencies of the tower without water are considered in analysis types I and II and are given in Figs. 15. Soil flexibility is included using the same stiffness coefficients as in Example 1, yielding to the first four mode shapes and corresponding vibration frequencies presented in Fig. 16.

Analysis types I and II as well as the reference solution are used to compute hydrodynamic pressure at Point A and the horizontal acceleration and displacement along x -direction at Point B as illustrated in Fig. 14. The obtained time-histories are nondimensionalized using the same factors as in Example 1. Figs. 17 and 18 show the obtained results for a rigid and flexible soil foundation, respectively. Although the agreement between analysis type I and the reference solution is still very satisfactory, there is a slight difference which originates mainly from the dissimilarity between higher mode frequencies predicted by the Euler-Bernoulli beam-based analytical formulation pre-

sented in Section 2.3 and those from 3D solid finite elements, as illustrated in Figs. 15 and 16. Figs. 17 and 18 also reveal that analysis type II gives excellent results when compared to the reference solution for both rigid and flexible soil conditions.

3.3 Example 3: Composite axisymmetric structure with a mass on top

In this example, we investigate the dynamic response of the structure illustrated in Fig. 19 (a): a composite axisymmetric tower, i.e. several constitutive materials, with a non-uniform cross-section, i.e. irregular interior wall. The inhomogeneous and irregular characters of the structure prevent the application of analysis type I, therefore only results of analysis type II and the reference solution are described next. The tower has the same exterior dimensions as in Example 2 while having an irregular interior wall as indicated in Fig. 19 (a). It is made of five materials, with the mechanical properties presented in Table 1.

The structure is surrounded by an infinite water domain as indicated in Fig. 19 (b). Water is assumed compressible, with the same properties as in the previous examples. The effects of surface gravity waves are neglected. The same earthquake input as in the previous examples is applied. Fig. 21 shows the finite element model of the tower without water, as well as the coupled 3D finite element model of the tower-water system constructed to obtain the reference solution. A constant modal damping ratio $\xi = 5\%$ is assigned to all the modes included in the analysis and both rigid and flexible soil assumptions are considered as previously. Soil flexibility is considered using the same properties as in Example 1. The first four modes of the tower without water are included in analysis type II. They are illustrated as well as the corresponding vibration frequencies for both rigid and flexible soil foundation in Figs. 20 (a) and (b), respectively.

Hydrodynamic pressure at Point A and the horizontal acceleration and displacement along x -direction at Point B illustrated in Fig. 21 are computed and nondimensionalized as described in the previous examples. Figs. 22 and 23 compare the reference solutions to the results of proposed analysis type II for rigid and flexible underlying soil foundations, respectively. It is seen that both types of results are almost identical, which confirms the high performance of the proposed analysis type II in determining the seismic response of towers with complex geometrical and material configurations, while enhancing the efficiency of the analysis process by waiving the need for coupled finite element solutions and associated discretization of the surrounding water domain.

3.4 Example 4: Frequency response functions and vibration periods of the studied tower-water systems

The results shown in the previous examples focused on the time-history responses of tower-water systems subjected to an earthquake. In this example, we verify the ability of the procedures developed to evaluate the frequency response and vibration periods of the tower-water systems described in the previous examples. For each case, analysis type II is applied to determine frequency response functions for horizontal acceleration at point B through Eq. (60). A frequency range from 0 to 10 Hz

is considered. Fig. 24 compares the acceleration frequency response functions \bar{u} obtained using the proposed technique under the effect of a unit harmonic exciting ground acceleration $\ddot{u}_g(t) = e^{i\omega t}$ to those from coupled finite element models of the tower-water systems described in Examples 1 to 3. The very good agreement between both methods confirms the validity of the proposed procedure in predicting dynamic response in the frequency domain. The curves also illustrate the shift towards lower frequencies due to soil flexibility. The assessment of coupled vibration periods is also an important step for structural seismic analysis and safety evaluation. These vibration periods can be determined as the resonances on the frequency response curves. Fig. 25 compares the first three vibration periods obtained for each of the three axisymmetric towers to those given by the coupled finite element models. We can clearly observe the excellent agreement with finite element solutions independently of the case studied.

3.5 Example 5: Effects of surface gravity waves on the dynamic response of the studied tower-water systems

The equations presented Section 2.5 are applied next to illustrate the effects of surface gravity waves on the dynamic response of the six tower-water systems studied previously. Fig. 26 presents the nondimensionalized hydrodynamic pressure frequency response functions $\bar{p}/(\rho_w g H_w)$ obtained at three points of the structure-water interface, located at $z = 6$ m, $z = 26$ m and $z = 28$ m above the heel of each tower. A low frequency range from 0 to 3 Hz is considered for better visualization of the response curves. Comparison of the results with and without surface gravity waves reveals that the effects on hydrodynamic pressure are: (i) mainly concentrated at the low frequency range, i.e. frequencies less than 0.5 Hz, and (ii) are more important closer to water surface. It can also be seen that hydrodynamic pressures in flexible foundation tower-water systems, i.e. lower coupled vibration frequencies, are more sensitive to surface gravity waves than those with rigid foundations. Fig. 27 shows the nondimensionalized hydrodynamic force frequency response functions $\bar{f}/(\rho_w g H_w^2)$ obtained for the six tower-water systems studied, where \bar{f} is determined by integrating hydrodynamic pressure \bar{p} over water depth. These results confirm that the effects of surface gravity waves on hydrodynamic loads are limited to the low frequency range. The same conclusion applies to the influence on dynamic structural response as can be seen from Figure 28 illustrating frequency response functions for horizontal acceleration \bar{u} obtained at point B of each of the towers.

4 Conclusions

In this paper, we developed original and efficient analysis procedures to determine the dynamic response of axisymmetric structures vibrating in contact with water. Two types of formulations were proposed: (i) Type I, where the mode shapes of the dry structure, i.e. without water, are obtained using analytical expressions based on Euler-Bernoulli beam theory, and (ii) Type II, where these modes shapes are extracted from a finite element analysis. Both formulations take account of higher vibration modes, water compressibility, flexibility of underlying soil foundation and surface gravity waves. Formulation type II further applies to composite axisymmetric structures made of different

materials, i.e. variation of stiffness and mass density along structure's height, as well as those with non-uniform hollow cross-sections due to geometric irregularity of the interior wall. Flowcharts illustrating the application of the proposed procedures were provided to facilitate practical programming. Illustrative examples of homogeneous and composite towers laying on rigid and flexible soil foundations were proposed and examined to illustrate the application of the proposed techniques and assess their efficiency. The results of the proposed methods were successfully validated against those from coupled tower-water finite element solutions built for this purpose. Analysis type II was shown to be more efficient in determining the dynamic and seismic response of axisymmetric structures with complex geometrical and material configurations. The effects of surface gravity waves on the dynamic response of the studied tower-systems were also discussed. The proposed techniques constitute interesting alternatives to more conventional methods since they: (i) can be easily programmed as illustrated by the flowcharts provided, (ii) include several analysis parameters such as material inhomogeneity, geometrical irregularity, higher mode effects, and soil conditions, (iii) enhance the efficiency of the analysis process by waiving the need for coupled finite element or boundary element solutions and required discretization of the surrounding water domain.

Acknowledgements

The authors would like to acknowledge the financial support of the Quebec Fund for Research on Nature and Technology (FRQNT). The research was also partly supported by Kwang-Hua Fund for College of Civil Engineering, Tongji University and the National Science Foundation of China, Grant No. 51278376 and No. 90915011.

Appendix A: Expressions for Hydrodynamic Frequency Response Functions

The analytical expressions for hydrodynamic pressure are reviewed in this appendix. By solving Eq. (1) under boundary conditions (2) to (5), Liaw and Chopra (1974) proposed the following expressions for frequency response functions \bar{p}_0 and \bar{p}_j , $j = 1 \dots N_s$

$$\bar{p}_0(R_s, \theta, z, \omega) = \frac{4\rho_w}{H_w} \left[- \sum_{n=1}^{\bar{n}-1} \frac{I_{0n}}{\kappa_n} \mathcal{D}_n(\kappa_n R_s) \cos(\lambda_n z) e^{i\tau_n R_s} + \sum_{n=\bar{n}}^{N_w} \frac{I_{0n}}{\kappa'_n} \mathcal{E}_n(\kappa'_n R_s) \cos(\lambda_n z) \right] \cos(\theta) \quad (\text{A1})$$

$$\bar{p}_j(R_s, \theta, z, \omega) = \frac{4\rho_w}{H_w} \left[- \sum_{n=1}^{\bar{n}-1} \frac{I_{jn}}{\kappa_n} \mathcal{D}_n(\kappa_n R_s) \cos(\lambda_n z) e^{i\tau_n R_s} + \sum_{n=\bar{n}}^{N_w} \frac{I_{jn}}{\kappa'_n} \mathcal{E}_n(\kappa'_n R_s) \cos(\lambda_n z) \right] \cos(\theta) \quad (\text{A2})$$

where N_w is the number of considered acoustical water modes, and the parameters λ_n , κ_n , κ'_n , I_{0n} , I_{jn} , \mathcal{D}_n , \mathcal{E}_n and τ_n are given by

$$\lambda_n = \frac{(2n-1)\pi}{2H_w}; \quad \kappa_n = \sqrt{\frac{\omega^2}{C_w^2} - \lambda_n^2}; \quad \kappa'_n = -i\kappa_n \quad (\text{A3})$$

$$I_{0n} = -\frac{2H_w(-1)^n}{\pi(2n-1)}; \quad I_{jn} = \int_0^{H_w} \psi_j^{(x)}(z) \cos(\lambda_n z) dz \quad (\text{A4})$$

$$\mathcal{D}_n(\kappa_n R_s) = \sqrt{\frac{[\mathbf{J}_1(\kappa_n R_s)]^2 + [\mathbf{Y}_1(\kappa_n R_s)]^2}{[\mathbf{J}_0(\kappa_n R_s) - \mathbf{J}_2(\kappa_n R_s)]^2 + [\mathbf{Y}_0(\kappa_n R_s) - \mathbf{Y}_2(\kappa_n R_s)]^2}} \quad (\text{A5})$$

$$\mathcal{E}_n(\kappa'_n R_s) = \frac{\mathbf{K}_1(\kappa'_n R_s)}{\mathbf{K}_0(\kappa'_n R_s) + \mathbf{K}_2(\kappa'_n R_s)} \quad (\text{A6})$$

$$\tau_n R_s = \tan^{-1} \left\{ \frac{[\mathbf{Y}_0(\kappa_n R_s) - \mathbf{Y}_2(\kappa_n R_s)] \mathbf{J}_1(\kappa_n R_s) - [\mathbf{J}_0(\kappa_n R_s) - \mathbf{J}_2(\kappa_n R_s)] \mathbf{Y}_1(\kappa_n R_s)}{[\mathbf{J}_0(\kappa_n R_s) - \mathbf{J}_2(\kappa_n R_s)] \mathbf{J}_1(\kappa_n R_s) + [\mathbf{Y}_0(\kappa_n R_s) - \mathbf{Y}_2(\kappa_n R_s)] \mathbf{Y}_1(\kappa_n R_s)} \right\} \quad (\text{A7})$$

in which \mathbf{K}_ℓ is the modified Bessel function of order ℓ of the second kind and \mathbf{J}_ℓ and \mathbf{Y}_ℓ are the Bessel functions of order ℓ of the first and second kind, respectively. The integer \bar{n} in the first sums of Eqs. (A1) and (A2) is the smallest value of integer n such that $\lambda_n > \frac{\omega}{C_w}$. We note that the first series in Eqs. (A1) and (A2) vanishes if $\bar{n} = 1$.

If water is assumed incompressible, the frequency-independent hydrodynamic pressure solutions \bar{p}_0 and \bar{p}_j given by Eq. (A1) and (A2) can be simplified to

$$\bar{p}_0(R_s, z, \theta, \omega) = \sum_{n=1}^{N_w} \bar{p}_{0n}(R_s, z, \theta, \omega) \quad (\text{A8})$$

$$\bar{p}_j(R_s, z, \theta, \omega) = \sum_{n=1}^{N_w} \bar{p}_{jn}(R_s, z, \theta, \omega) \quad (\text{A9})$$

with

$$\bar{p}_{0n}(R_s, z, \theta, \omega) = \frac{4\rho_w I_{0n}}{H_w \kappa'_n} \mathcal{E}_n(\kappa'_n R_s) \cos(\lambda_n z) \cos(\theta) \quad (\text{A10})$$

$$\bar{p}_{jn}(R_s, z, \theta, \omega) = \frac{4\rho_w I_{jn}}{H_w \kappa'_n} \mathcal{E}_n(\kappa'_n R_s) \cos(\lambda_n z) \cos(\theta) \quad (\text{A11})$$

in which λ_n , I_{0n} , I_{jn} and $\mathcal{E}_n(\kappa'_n R_s)$ are still given by Eqs. (A3), (A4) and (A6), while

$$\kappa'_n = \frac{(2n-1)\pi}{2H_w} \quad (\text{A12})$$

When the effects of surface gravity waves are to be included in the analysis, Liaw and Chopra (1974) solved the wave equation (1) considering the boundary condition in Eq. (55) and showed that hydrodynamic pressure frequency response functions \bar{p}_0 and \bar{p}_j , $j = 1 \dots N_s$, can be expressed as

$$\begin{aligned} \bar{p}_0(R_s, \theta, z, \omega) = 8\rho_w \Big[& -\frac{\lambda_0}{\kappa_0} \frac{I_{00}}{[2\lambda_0 H_w + \sinh(2\lambda_0 H_w)]} \mathcal{D}_0(\kappa_0 R_s) \cosh(\lambda_0 z) e^{i\tau_0 R_s} \\ & - \sum_{n=1}^{\bar{n}-1} \frac{\lambda_n}{\kappa_n} \frac{I_{0n}}{[2\kappa_n H_w + \sin(2\lambda_n H_w)]} \mathcal{D}_n(\kappa_n R_s) \cos(\lambda_n z) e^{i\tau_n R_s} \\ & + \sum_{n=\bar{n}}^{N_w} \frac{\lambda_n}{\kappa'_n} \frac{I_{0n}}{[2\kappa'_n H_w + \sin(2\lambda_n H_w)]} \mathcal{E}_n(\kappa'_n R_s) \cos(\lambda_n z) \Big] \cos(\theta) \end{aligned} \quad (\text{A13})$$

$$\begin{aligned} \bar{p}_j(R_s, \theta, z, \omega) = 8\rho_w \Big[& -\frac{\lambda_0}{\kappa_0} \frac{I_{j0}}{[2\lambda_0 H_w + \sinh(2\lambda_0 H_w)]} \mathcal{D}_n(\kappa_n R_s) \cosh(\lambda_n z) e^{i\tau_n R_s} \\ & - \sum_{n=1}^{\bar{n}-1} \frac{\lambda_n}{\kappa_n} \frac{I_{jn}}{[2\kappa_n H_w + \sin(2\lambda_n H_w)]} \mathcal{D}_n(\kappa_n R_s) \cos(\lambda_n z) e^{i\tau_n R_s} \\ & + \sum_{n=\bar{n}}^{N_w} \frac{\lambda_n}{\kappa'_n} \frac{I_{jn}}{[2\kappa'_n H_w + \sin(2\lambda_n H_w)]} \mathcal{E}_n(\kappa'_n R_s) \cos(\lambda_n z) \Big] \cos(\theta) \end{aligned} \quad (\text{A14})$$

where N_w is the number of considered acoustical water modes and the parameters κ'_n , I_{jn} , \mathcal{D}_n , \mathcal{E}_n and τ_n are given by the same equations as previously, while the parameters λ_0 and λ_n are now solutions of the following two equations, respectively

$$\lambda_0 \tanh(\lambda_0 H_w) = \frac{\omega^2}{g} \quad (\text{A15})$$

$$\lambda_n \tan(\lambda_n H_w) = -\frac{\omega^2}{g}; \quad n = 1 \dots N_w \quad (\text{A16})$$

and the parameters κ_0 , κ_n , I_{00} , I_{0n} , and I_{j0} are given by

$$\kappa_0 = \sqrt{\frac{\omega^2}{C^2} + \lambda_0^2} \quad (\text{A17})$$

$$\kappa_n = \sqrt{\frac{\omega^2}{C^2} - \lambda_n^2}; \quad n = 1 \dots N_w \quad (\text{A18})$$

$$I_{00} = \int_0^{H_w} \cosh(\lambda_0 z) \, dz = \frac{\sinh(\lambda_0 H_w)}{\lambda_0} \quad (\text{A19})$$

$$I_{j0} = \int_0^{H_w} \psi_j^{(x)}(z) \cosh(\lambda_0 z) \, dz; \quad j = 1 \dots N_s \quad (\text{A20})$$

$$I_{0n} = \int_0^{H_w} \cos(\lambda_n z) \, dz = \frac{\sin(\lambda_n H_w)}{\lambda_n}; \quad n = 1 \dots N_w \quad (\text{A21})$$

As previously, the integer \bar{n} in the second sums of Eqs. (A13) and (A14) denotes the smallest value of integer n such that $\lambda_n > \frac{\omega}{C_w}$.

References

- ADINA Theory and Modeling Guide. Report ARD 10-7. ADINA R & D, Inc.; 2014.
- Auciello NM. Transverse vibrations of a linearly tapered cantilever beam with tip mass of rotatory inertia and eccentricity. *J Sound Vibr* 1996;194:25-34.
- Bartrop NDP, Adams AJ. Dynamics of fixed marine structures. 3rd ed. Oxford: Butterworth-Heinemann; 1991.
- Bouaanani N, Lu FY. Assessment of potential-based fluid finite elements for seismic analysis of dam-reservoir systems. *J Comput Struct* 2009;87:206-24.
- Bouaanani N, Perrault C. Practical formulas for frequency domain analysis of earthquake-induced dam-reservoir interaction. *J Eng Mech ASCE* 2010;136:107-19.
- Chang JY, Liu WH. Some studies on the natural frequencies of immersed restrained column. *J Sound Vibr* 1989;130:516-24.
- Chen BF. Dynamic responses of coastal structures during earthquakes including sediment-sea-structure interaction. *Soil Dyn Earthq Eng* 2000;20:445-67.
- Clough RW, Penzien J. Dynamics of structures. 2nd ed. New York: McGraw-Hill; 1993.
- Czygan O, Von Estorff O. Fluid-structure interaction by coupling BEM and nonlinear FEM. *Eng Anal Bound Elem* 2002;26:773-9.
- Eatock Taylor R, Duncan PE. Fluid-induced inertia and damping in vibrating offshore structures. *Appl Ocean Res* 1980;2:3-12.
- Everstine GC. A symmetric potential formulation for fluid-structure interaction. *J Sound Vibr* 1981;79:157-60.
- Fenves G, Chopra AK. EAGD-84, a computer program for earthquake analysis of concrete gravity dams. Report No. UCB/EERC-84/11, University of California, Berkeley, California: 1984.
- Goyal A, Chopra AK. Earthquake analysis of intake-outlet towers including tower-water-foundation-soil interaction. *Earthq Eng Struct Dyn* 1989;18:325-44.
- Gutiérrez E, Primi S, Taucer F, Caperan P, Tirelli D, Mieres J et al. A wind turbine tower design based on the use of fibre-reinforced composites. Institute for the Protection and Security of the Citizen, European Laboratory for Structural Assessment (ELSA), Ispra (VA), Italy; 2003.
- Han SM, Benaroya H, Wei T. Dynamics of transversely vibrating beams using four engineering theories. *J Sound Vibr* 1999;225:935-88.
- Lamb H. Hydrodynamics. 6th ed. Cambridge Eng.: The Cambridge University Press; 1932.
- Li M, Zhang H, Guan H, Lin G. Three-dimensional investigation of wave-pile group interaction using the scaled boundary finite element method. Part I: Theoretical developments, *Ocean Engineering* 2013;64:174-184.

- Li M, Guan H, Zhang H, Liu J. Three-dimensional investigation of wave-pile group interaction using the scaled boundary finite element method. Part II: Application results, *Ocean Engineering* 2013;64:185-195.
- Liaw CY, Chopra AK. Dynamics of towers surrounded by water. *Earthq Eng Struct Dyn* 1974;3:33-49.
- Liu J, Lin G. Numerical modelling of wave interaction with a concentric cylindrical system with an arc-shaped porous outer cylinder, *European Journal of Mechanics B/Fluids* 2013;37:59-71.
- Lu JF, Jeng DS. Dynamic response of an offshore pile to pseudo-Stoney waves along the interface between a poroelastic seabed and seawater. *Soil Dyn Earthq Eng* 2010;30:184-201.
- Mathews JH. Numerical methods for mathematics, science, and engineering. 2nd ed. Englewood Cliffs, N.J.: Prentice Hall; 1992.
- MATLAB ®. The Mathworks, Inc., Natick, MA, USA, 2011.
- Meng XN, Zou ZJ. Wave interaction with a uniform porous cylinder of arbitrary shape, *Ocean Engineering* 2012;44:90-99.
- Michaltsos GT, Ermopoulos JC. Dynamic response of column bases. *Eng Struct* 2001;23:58-71.
- Millán MA, Young YL, Prévost JH. Seismic response of intake towers including dam-tower interaction. *Earthq Eng Struct Dyn* 2009;38:307-29.
- Miquel B, Bouaanani N. Practical dynamic analysis of structures laterally vibrating in contact with water. *J Comput Struct* 2011;89:2195-210.
- Nagaya K, Hai Y. Seismic response of underwater members of variable cross section. *J Sound Vibr* 1985;103:119-38.
- Olson LG, Bathe KJ. Analysis of fluid-structure interactions. a direct symmetric coupled formulation based on the fluid velocity potential. *J Comput Struct* 1985;21:21-32.
- Öz HR. Natural frequencies of an immersed beam carrying a tip mass with rotatory inertia. *J Sound Vibr* 2003;266:1099-108.
- Pacific Earthquake Engineering Research Center (PEER) - Strong Motion Database, <http://peer.berkeley.edu/smcat/>, Date accessed: 22 March 2011.
- Rashedi A, Sridhar I, Tseng KJ. Multi-objective material selection for wind turbine blade and tower: Ashby's approach. *Mater Design* 2012;37:521-532.
- Seica MV, Packer JA. FRP materials for the rehabilitation of tubular steel structures, for underwater applications. *Compos Struct* 2007;80:440-450.
- Sigrist J-F, Garreau S. Dynamic analysis of fluid-structure interaction problems with modal methods using pressure-based fluid finite elements. *Finite Elem Anal Des* 2007;43:287-300.
- Spyrakos CC, Xu C. Soil-structure-water interaction of intake-outlet towers allowed to uplift. *Soil Dyn Earthq Eng* 1997;16:151-9.

- Sun X, Huang D, Wu G. The current state of offshore wind energy technology development. *Energy* 2012;41:298-312.
- Tanaka Y, Hudspeth RT. Restoring forces on vertical circular cylinders forced by earthquakes. *Earthq Eng Struct Dyn* 1988;16:99-119.
- Tao L, Song H, Chakrabarti S. Scaled boundary FEM solution of short-crested wave diffraction by a vertical cylinder, *Computer Methods in Appl. Mech. and Eng.* 2007;197:232-242.
- Tricklebank AH, Halberstadt PH, Magee BJ. Concrete towers for onshore and offshore wind farms-conceptual design studies. Surrey: The Concrete Centre; 2007.
- Uściłowska A, Kołodziej JA. Free vibration of immersed column carrying a tip mass. *J Sound Vibr* 1998;216:147-57.
- Wei K, Yuan W, Bouaanani N, Chang C-C. An improved HSFR method for natural vibration analysis of an immersed cylinder pile with a tip mass. *Theor Appl Mech Lett* 2012;2:023002.
- Williams AN. Earthquake response of submerged circular cylinder. *Ocean Eng* 1986;13:569-85.
- Wu JS, Chen CT. An exact solution for the natural frequencies and mode shapes of an immersed elastically restrained wedge beam carrying an eccentric tip mass with mass moment of inertia. *J Sound Vibr* 2005;286:549-68.
- Xing JT, Price WG, Pomfret MJ, Yam LH. Natural vibration of a beam-water interaction system. *J Sound Vibr* 1997;199:491-512.

Table 1

Constitutive materials of the axisymmetric tower studied in Example 3.

	Mass density (kg/m ³)	Elastic modulus (GPa)	Poisson's ratio
Material 1	7850	210	0.3
Material 2	2400	35	0.2
Material 3	2500	25	0.2
Material 4	1900	50	0.2
Material 5	2400	30	0.2

List of figures

- Fig. 1: Examples of axisymmetric towers studied: (a) Cylindrical tower with uniform solid section; (b) Cylindrical tower with hollow uniform section; (c) Axisymmetric tower with non-uniform section and various constitutive materials along the height.
- Fig. 2: Approximation of parameters \mathcal{D}_n , \mathcal{E}_n and $\tau_n R_s$.
- Fig. 3: Approximation of the tower's structural mode shapes using polynomial functions.
- Fig. 4: Flowchart illustrating the proposed procedure based on analytical formulation of mode shapes, i.e. Analysis type I.
- Fig. 5: Flowchart illustrating the proposed procedure based on finite element determination of mode shapes, i.e. Analysis type II.
- Fig. 6: Cylindrical tower studied in Example 1.
- Fig. 7: Mode shapes included in the analysis of the cylindrical tower studied in Example 1.
- Fig. 8: Finite element models of the cylindrical tower studied in Example 1.
- Fig. 9: Time-histories of the seismic response of the axisymmetric tower studied in Example 1.
- Fig. 10: Mode shapes of the cylindrical tower studied in Example 1.
- Fig. 11: Time-histories of the seismic response of the axisymmetric tower studied in Example 1 including the effects of soil flexibility.
- Fig. 12: Axisymmetric tower studied in Example 2.
- Fig. 13: Finite element models of the axisymmetric tower studied in Example 2.
- Fig. 14: Mode shapes and corresponding frequencies of the axisymmetric tower studied in Example 2.
- Fig. 15: Mode shapes and corresponding frequencies of the axisymmetric tower studied in Example 2 including the effects of soil flexibility.
- Fig. 16: Time-histories of the seismic response of the axisymmetric tower studied in Example 2.
- Fig. 17: Time-histories of the seismic response of the axisymmetric tower studied in Example 2 including the effects of soil flexibility.

Fig. 18: Axisymmetric tower studied in Example 3: (a) Geometry of the axisymmetric tower; (b) Tower surrounded by an infinite water domain.

Fig. 19: Finite element mode shapes and corresponding frequencies of the composite axisymmetric tower studied in Example 3.

Fig. 20: Finite element models of the composite axisymmetric tower studied in Example 3.

Fig. 21: Time-histories of the seismic response of the composite axisymmetric tower studied in Example 3.

Fig. 22: Time-histories of the seismic response of the composite axisymmetric tower studied in Example 3 including the effects of soil flexibility.

Fig. 23: Frequency response functions for horizontal acceleration at point B of the tower-water systems studied.

Fig. 24: Vibration periods obtained using the reference and proposed solutions.

Fig. 25: Nondimensionalized hydrodynamic pressure frequency response functions $\bar{p}/(\rho_w g H_w)$ obtained at three points of the structure-water interface, located at $z = 6$ m, $z = 26$ m and $z = 28$ m above the heel of each tower.

Fig. 26: Nondimensionalized hydrodynamic force frequency response functions $\bar{f}/(\rho_w g H_w^2)$.

Fig. 27: Frequency response functions for horizontal acceleration \bar{u} at point B of the tower-water systems studied.

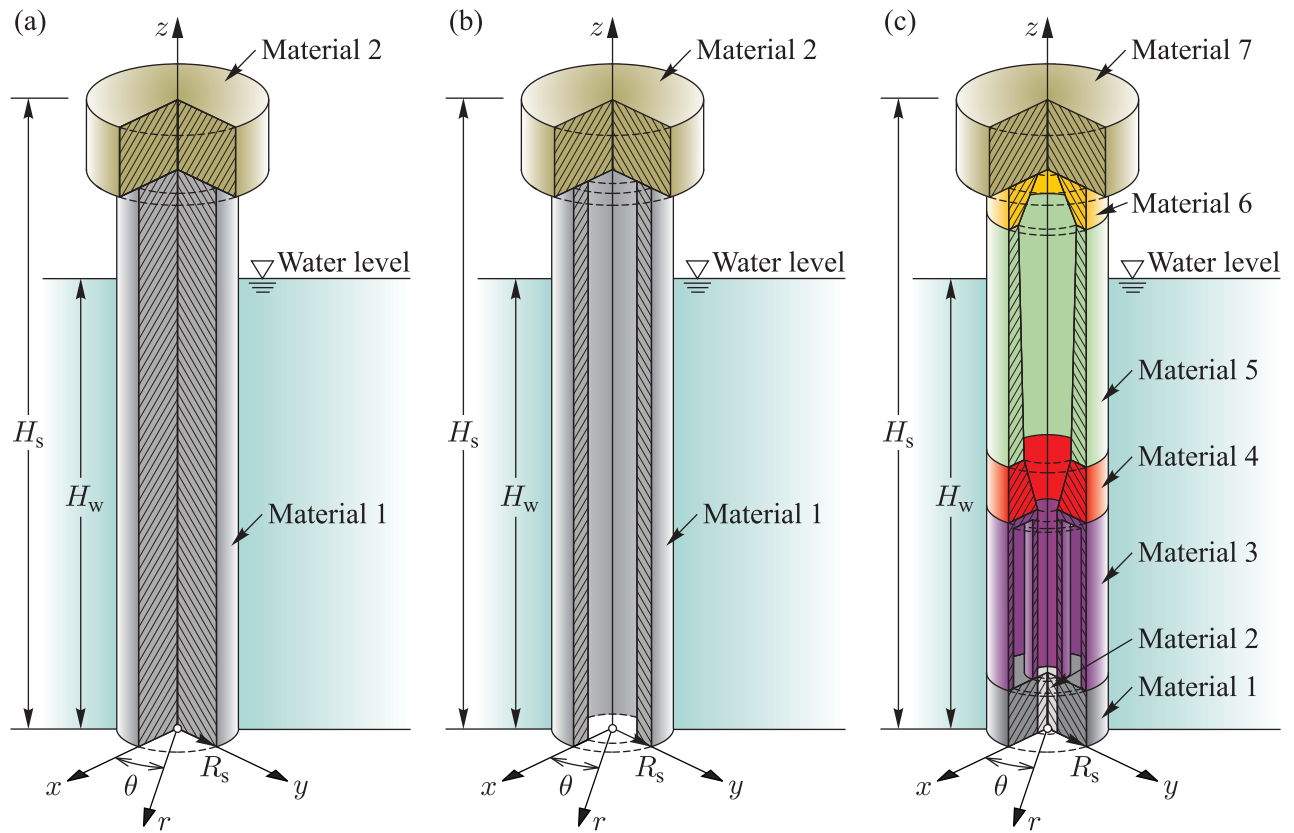


Figure 1. Examples of axisymmetric towers studied: (a) Cylindrical tower with uniform solid section; (b) Cylindrical tower with hollow uniform section; (c) Axisymmetric tower with non-uniform section and various constitutive materials along the height.

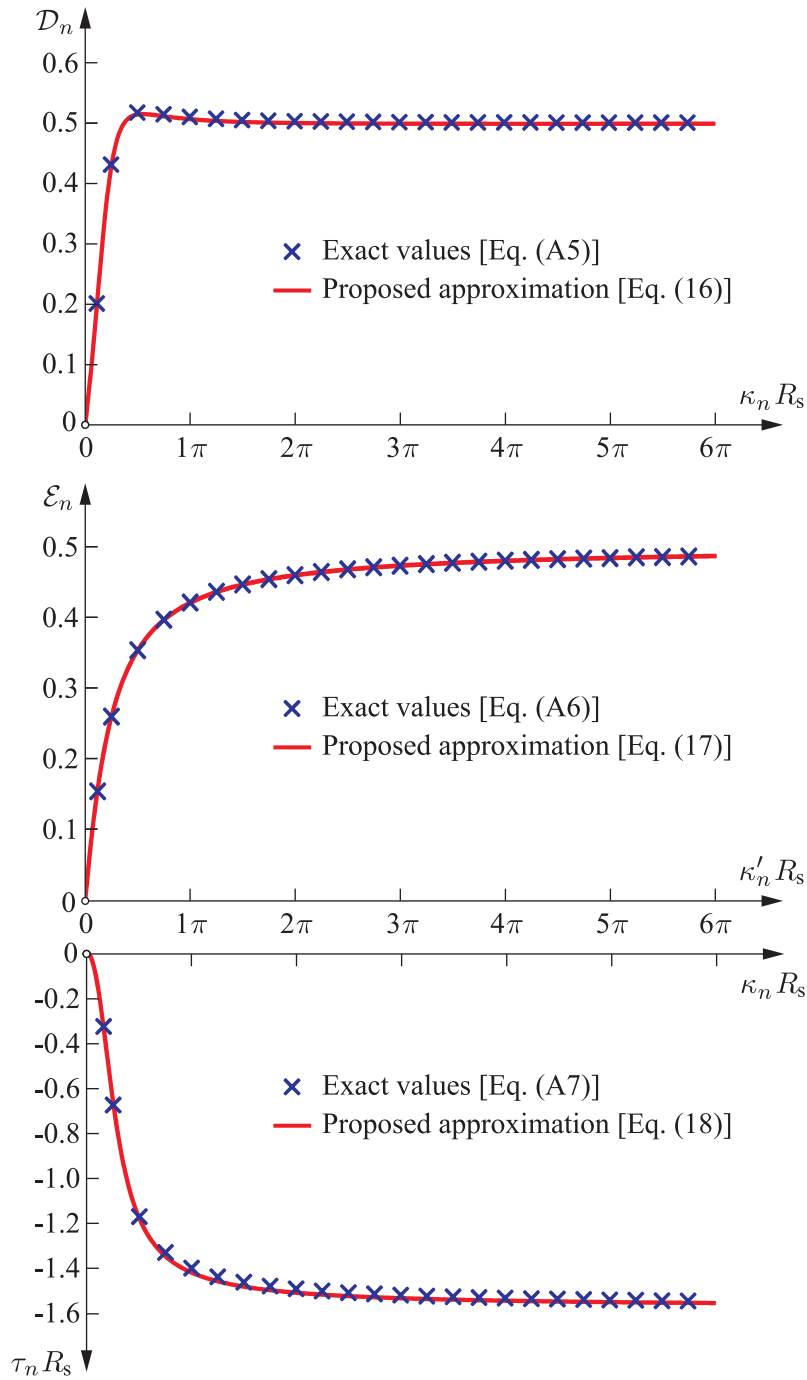


Figure 2. Approximation of parameters \mathcal{D}_n , \mathcal{E}_n and $\tau_n R_s$.

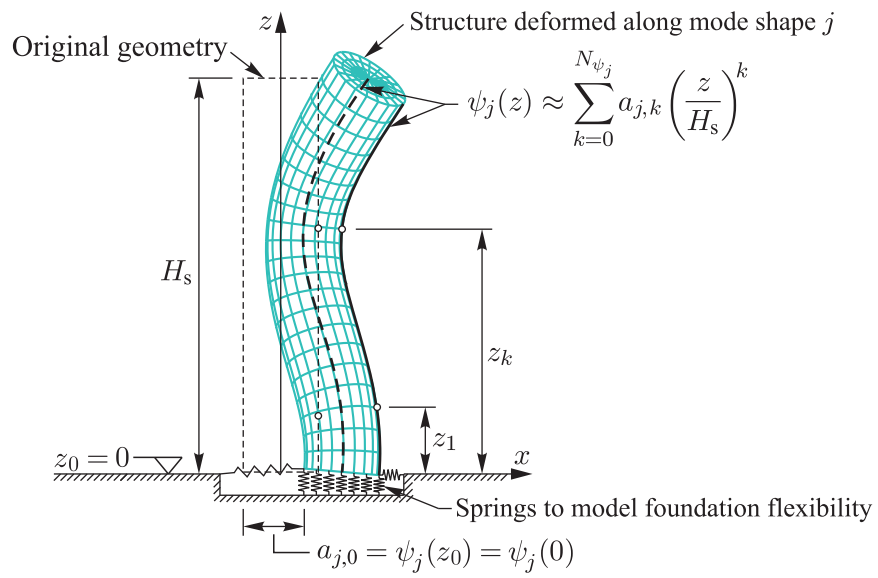


Figure 3. Approximation of the tower's structural mode shapes using polynomial functions.

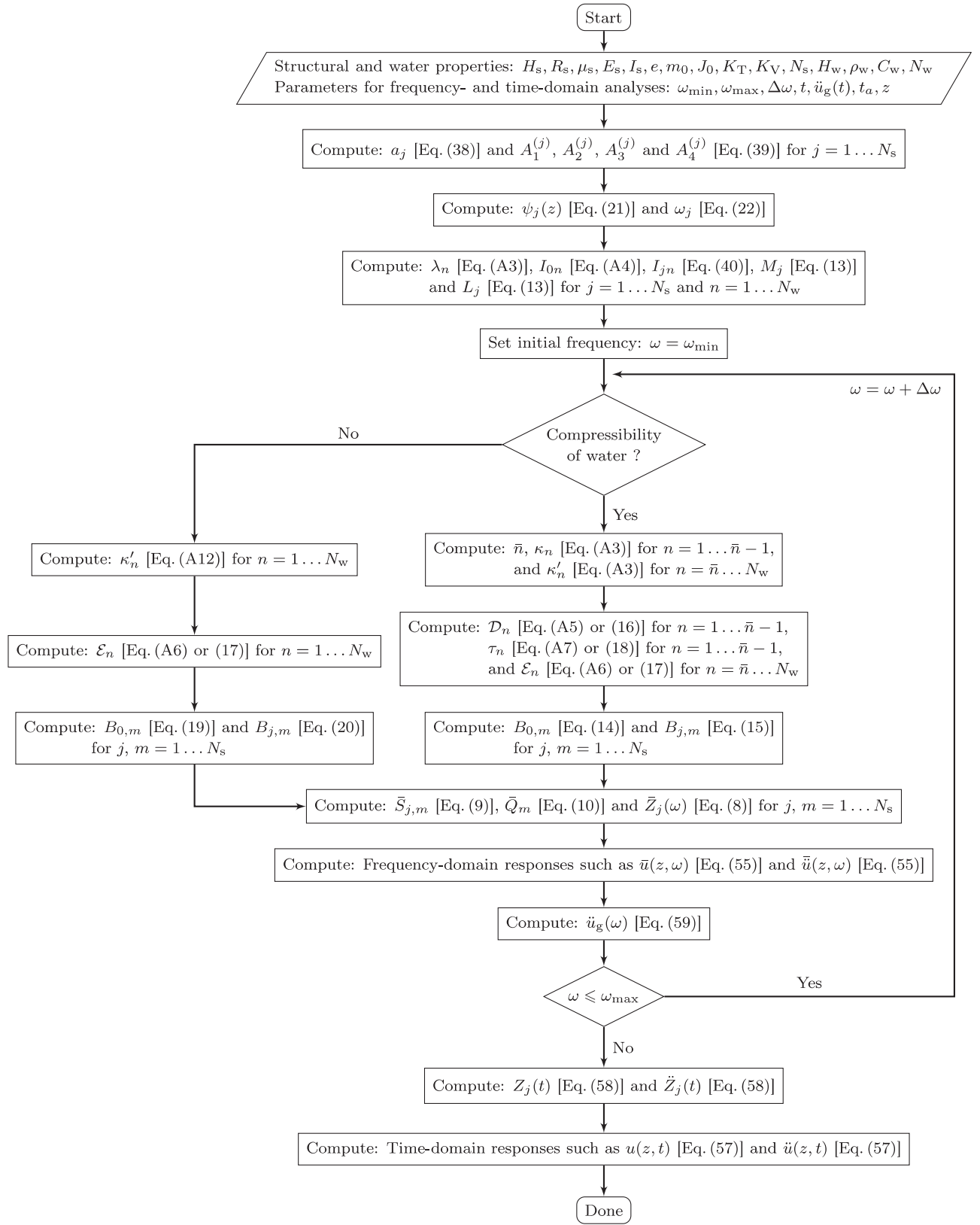


Figure 4. Flowchart illustrating the proposed procedure based on analytical formulation of mode shapes, i.e. Analysis type I.

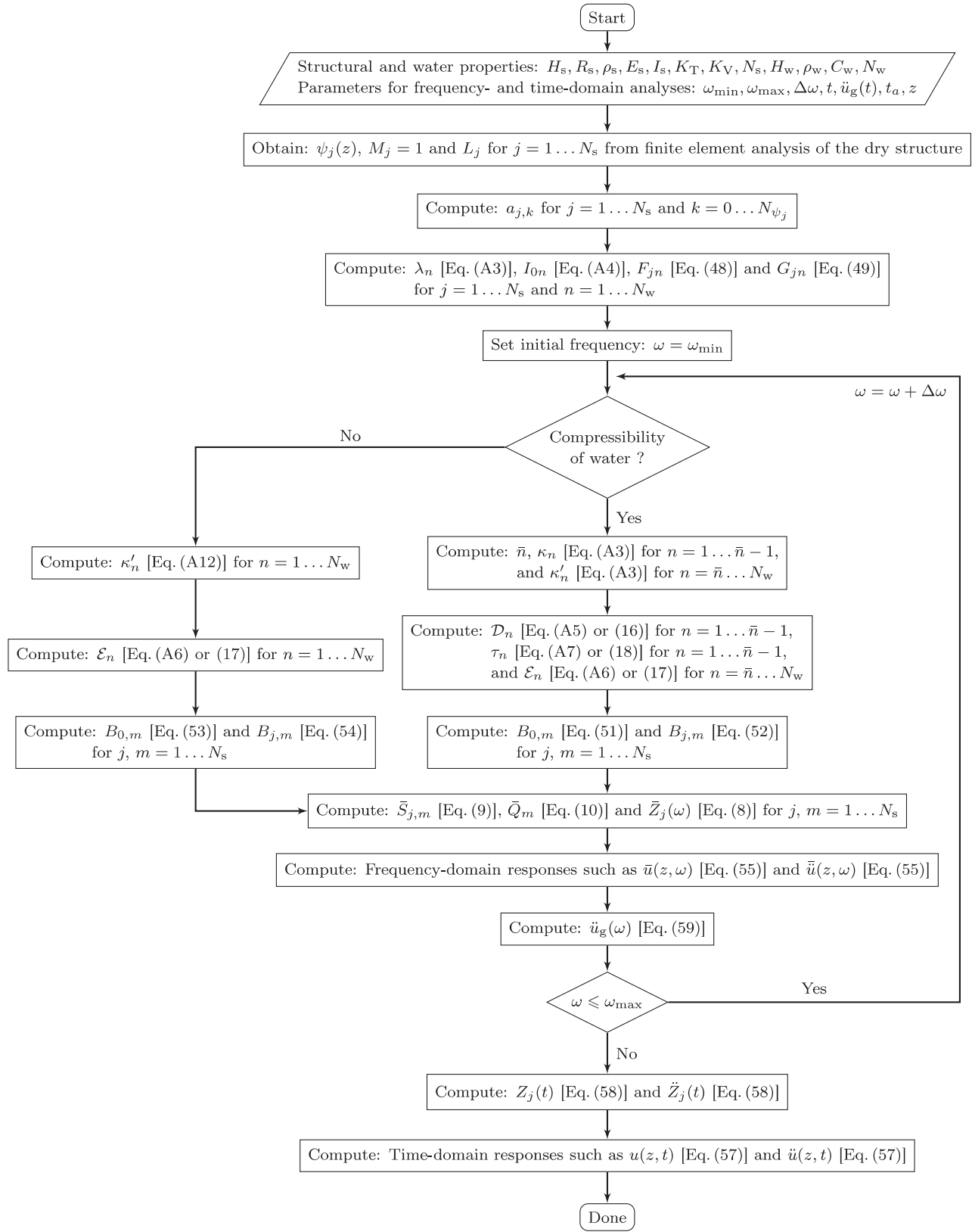


Figure 5. Flowchart illustrating the proposed procedure based on finite element determination of mode shapes, i.e. Analysis type II.

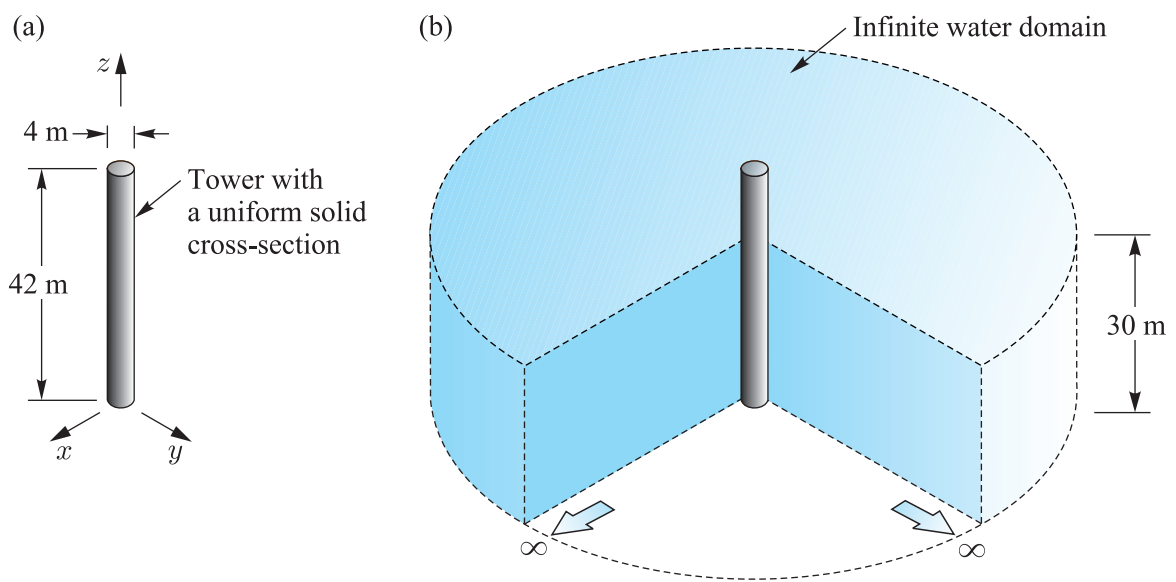


Figure 6. Cylindrical tower studied in Example 1: (a) Geometry of the cylindrical tower; (b) Tower surrounded by an infinite water domain.

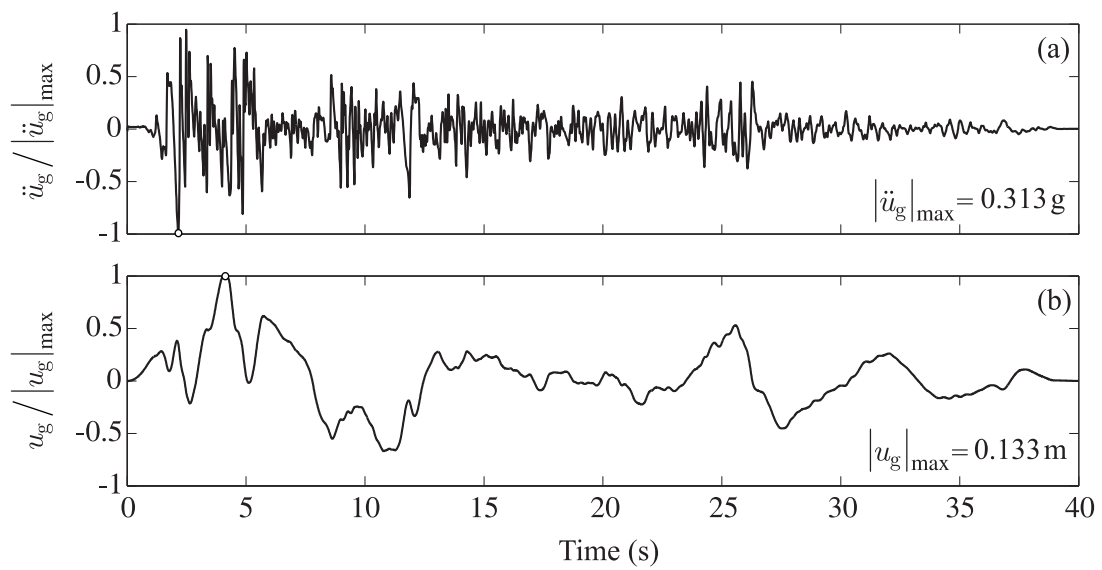


Figure 7. Imperial Valley earthquake horizontal N-S component at El Centro : (a) Accelerogram normalized by Peak Ground Acceleration PGA; (b) Displacement normalized by Peak Ground Displacement PGD.

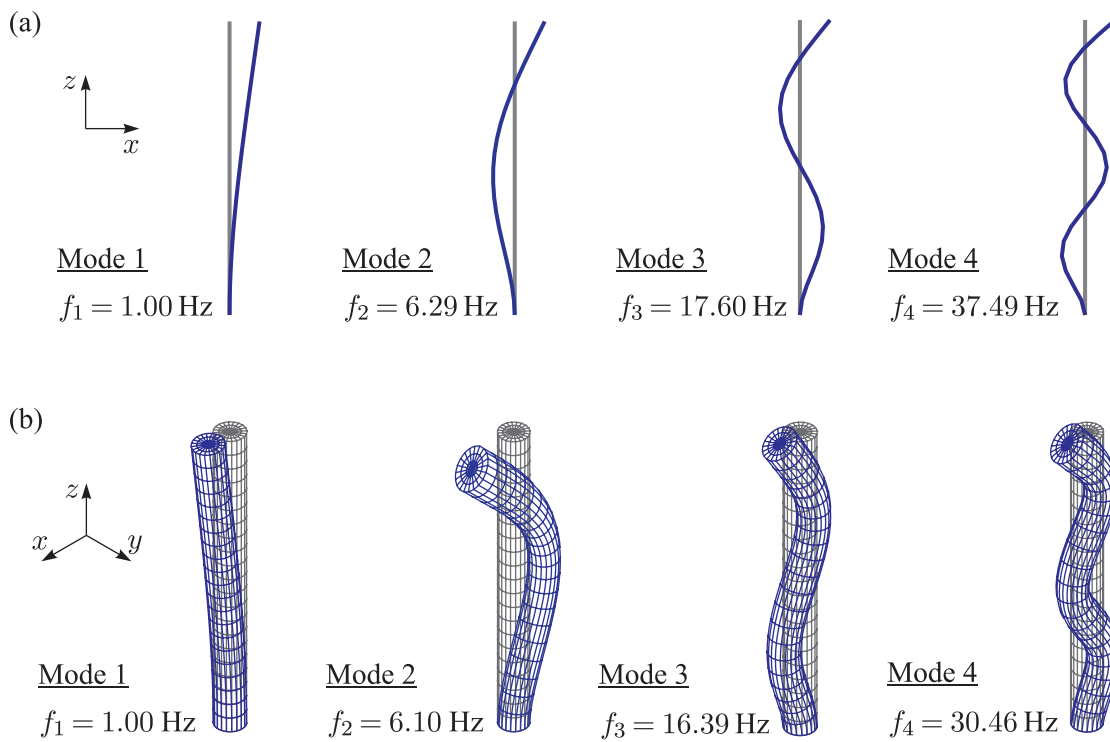


Figure 8. Mode shapes included in the analysis of the cylindrical tower studied in Example 1: (a) Analytical formulation; (b) Finite elements.

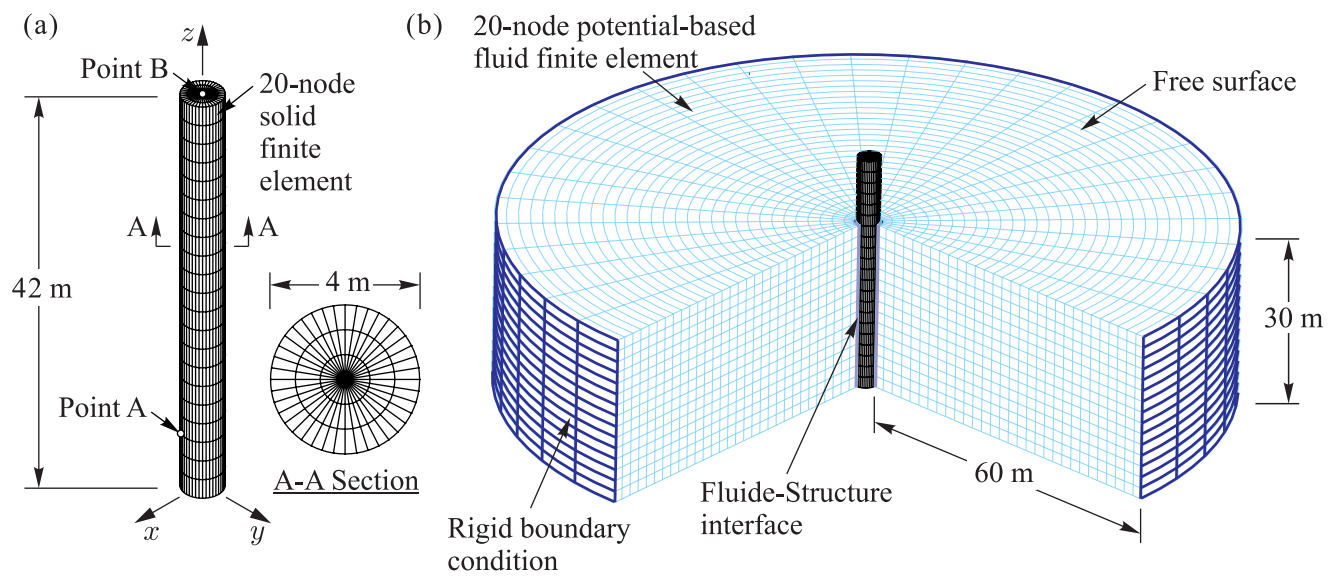


Figure 9. Finite element models of the cylindrical tower studied in Example 1: (a) Finite element model of the tower without water; (b) Finite element model of the coupled tower-water system.

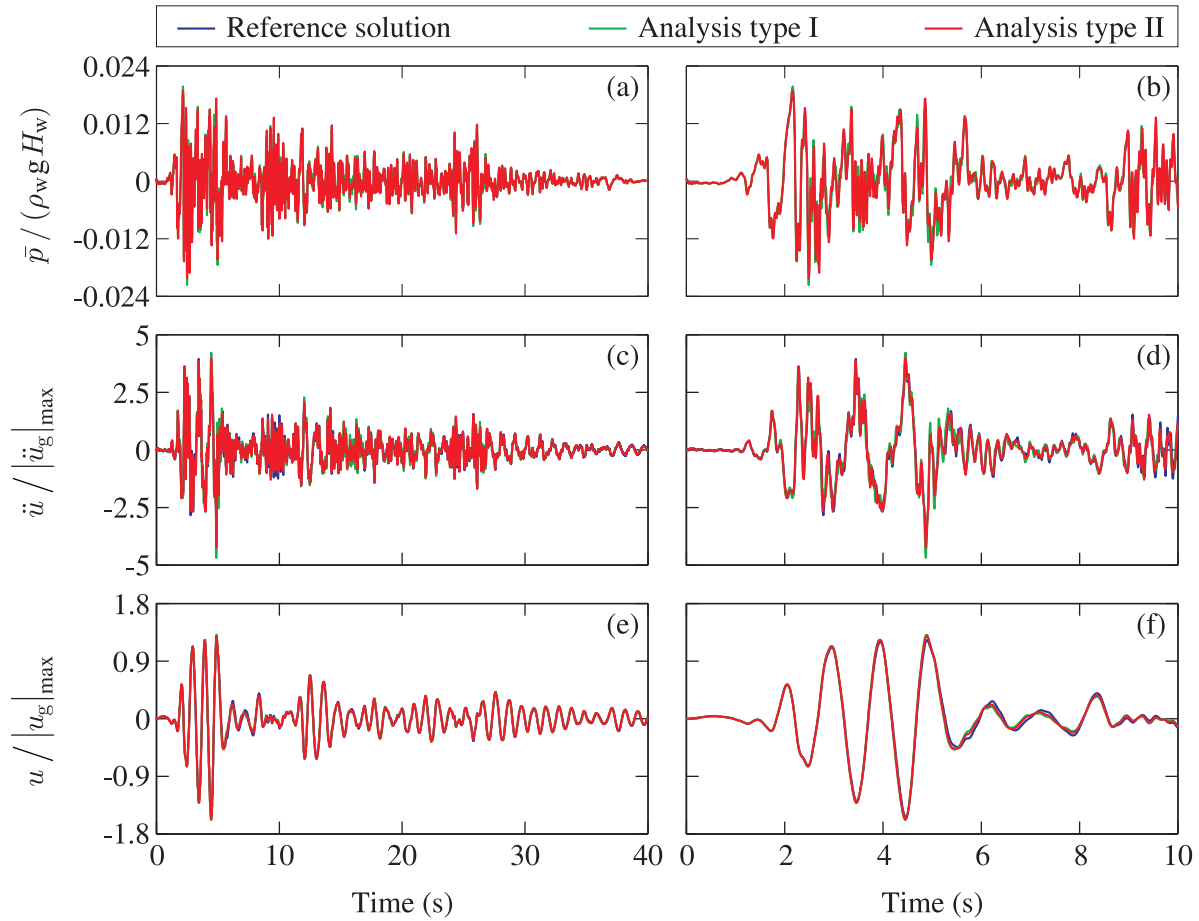


Figure 10. Time-histories of the seismic response of the axisymmetric tower studied in Example 1: (a) and (b) hydrodynamic pressure at point A; (c) and (d) horizontal acceleration at point B; (e) and (f) horizontal displacement at point B.

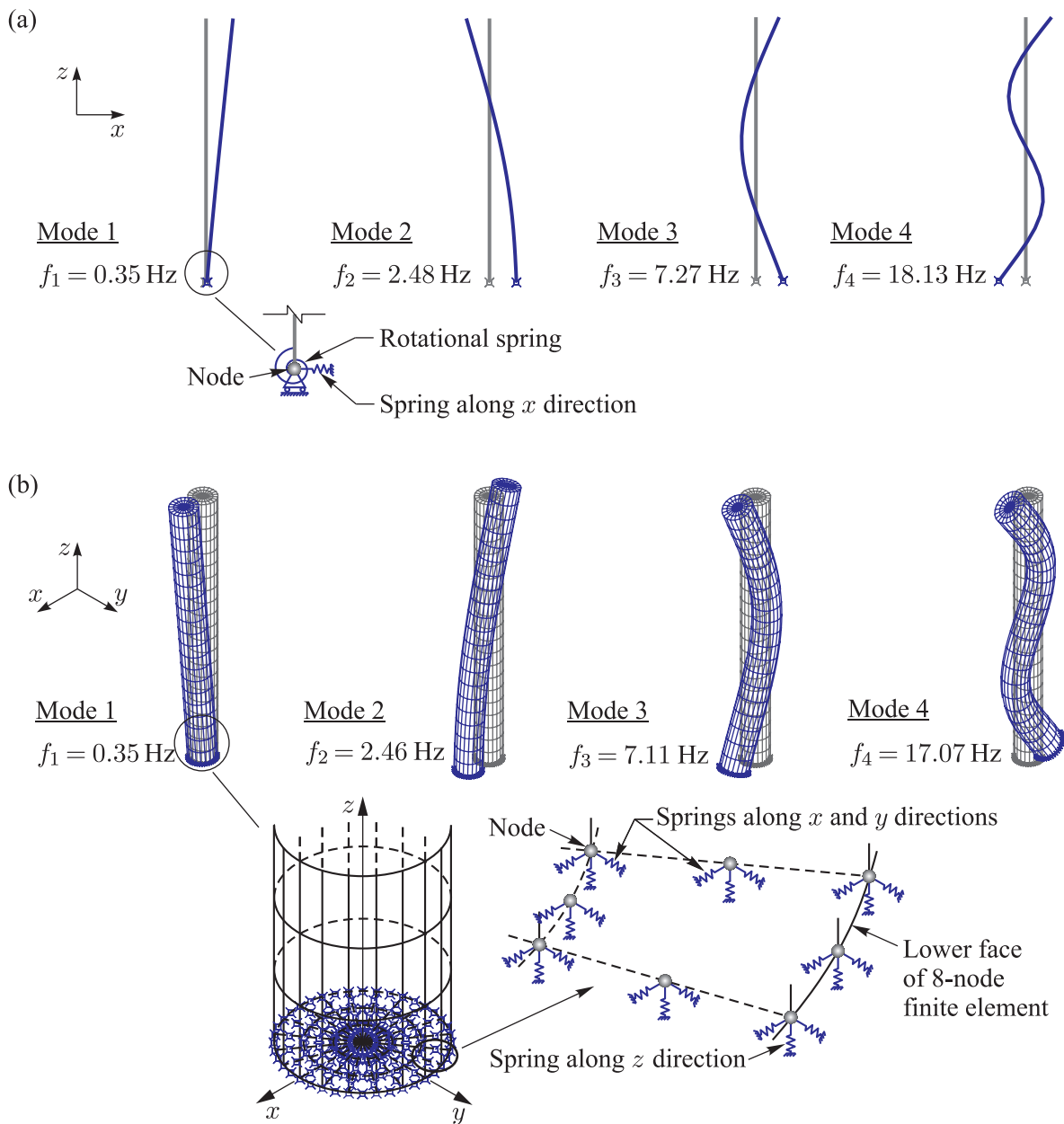


Figure 11. Mode shapes of the cylindrical tower studied in Example 1: (a) Analytical formulation; (b) Finite elements.

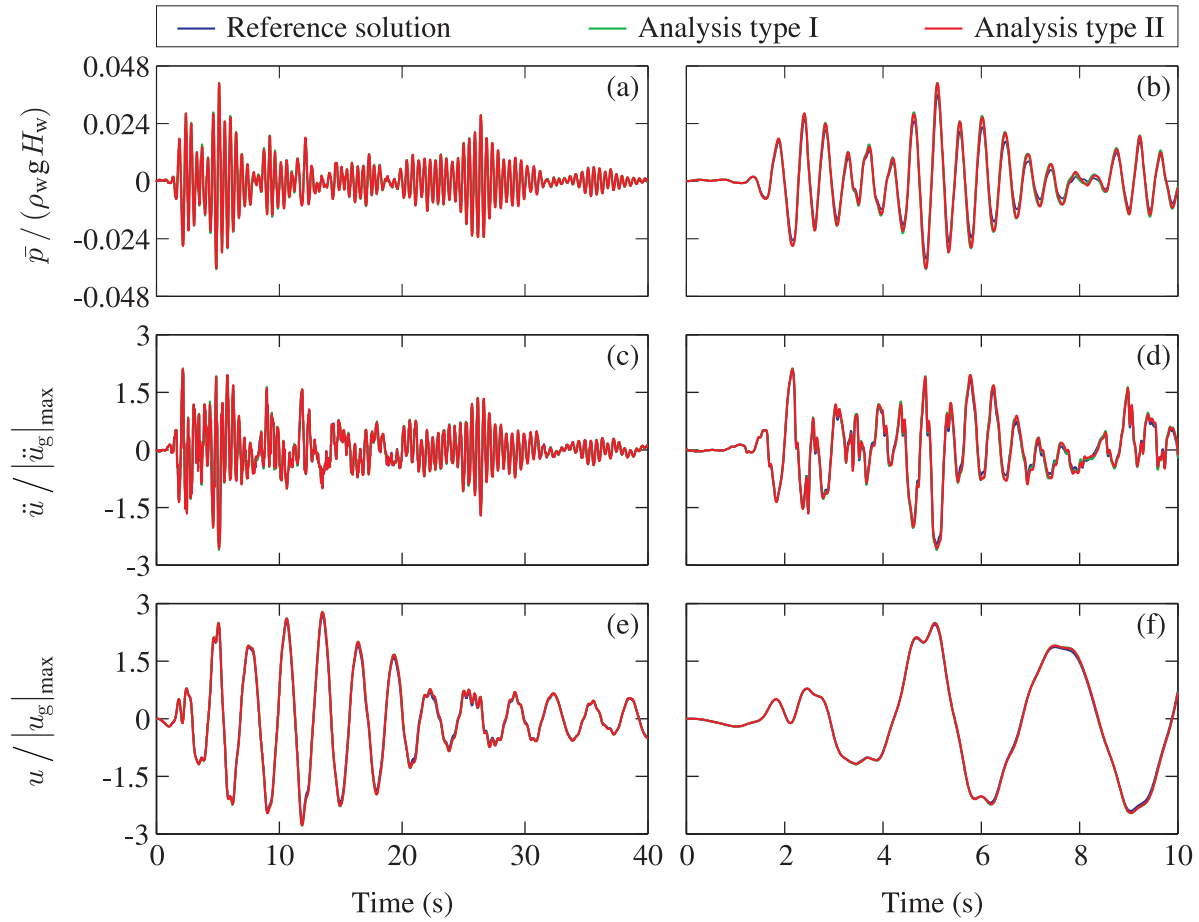


Figure 12. Time-histories of the seismic response of the axisymmetric tower studied in Example 1 including the effects of soil flexibility: (a) and (b) hydrodynamic pressure at point A; (c) and (d) horizontal acceleration at point B; (e) and (f) horizontal displacement at point B.

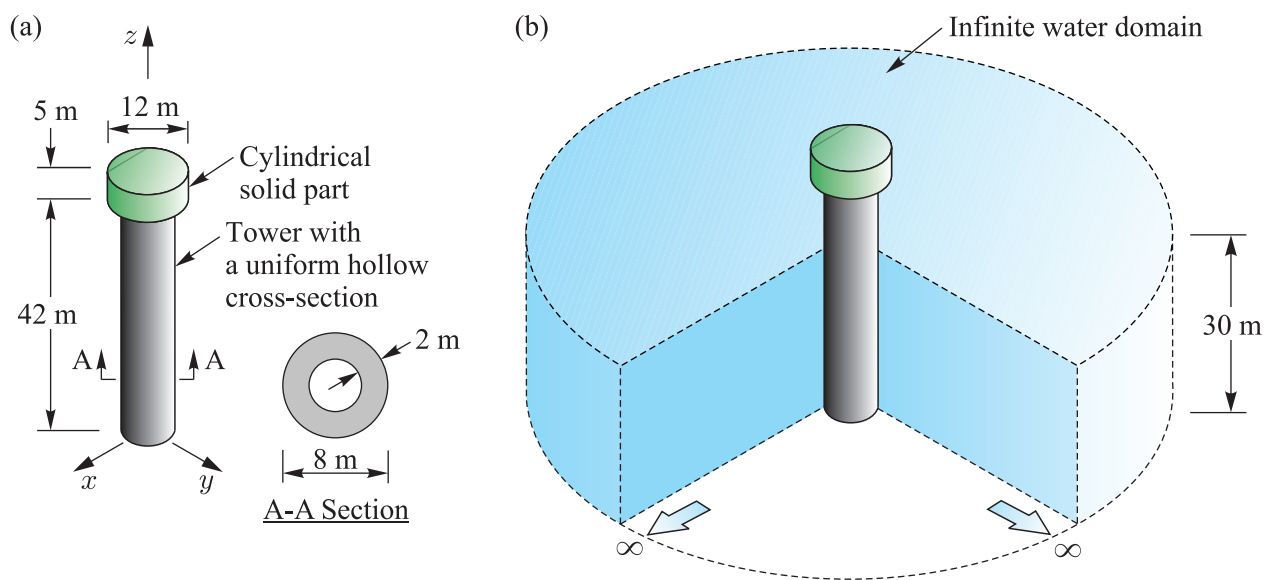


Figure 13. Axisymmetric tower studied in Example 2: (a) Geometry of the axisymmetric tower; (b) Tower surrounded by an infinite water domain.

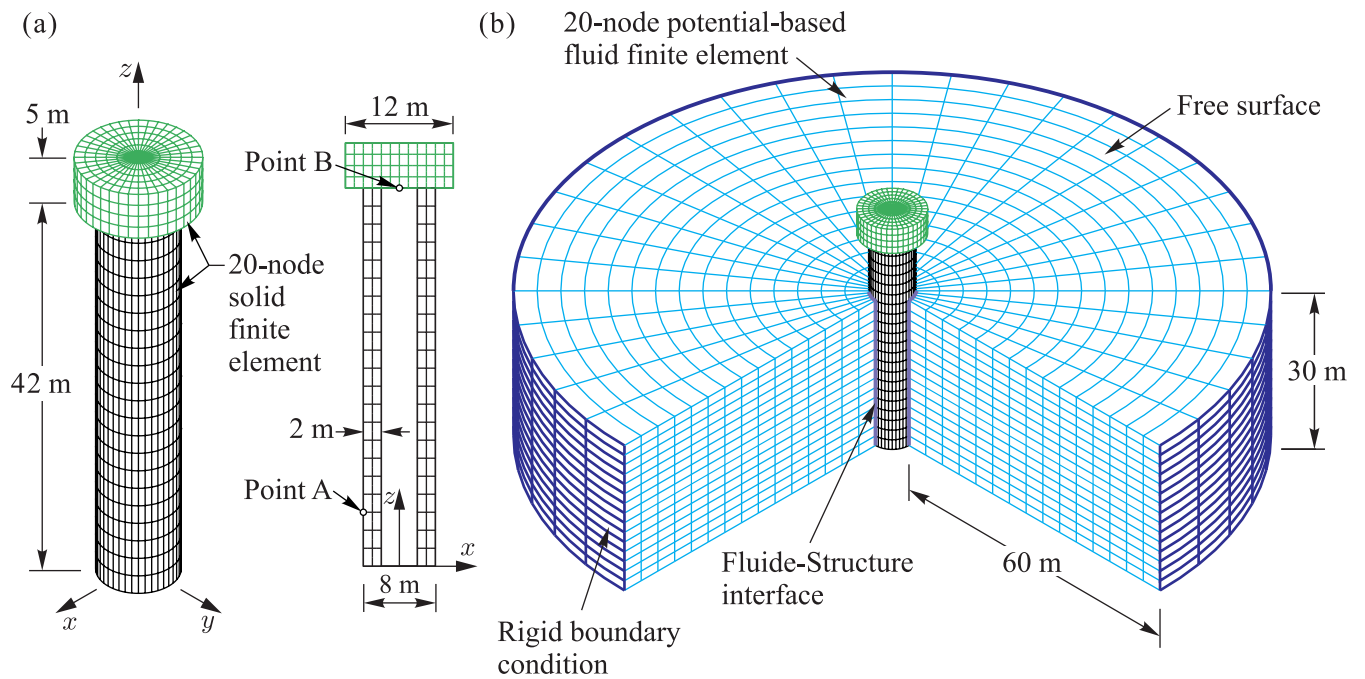


Figure 14. Finite element models of the axisymmetric tower studied in Example 2: (a) Finite element model of the structure without water; (b) Finite element model of the coupled tower-water system.

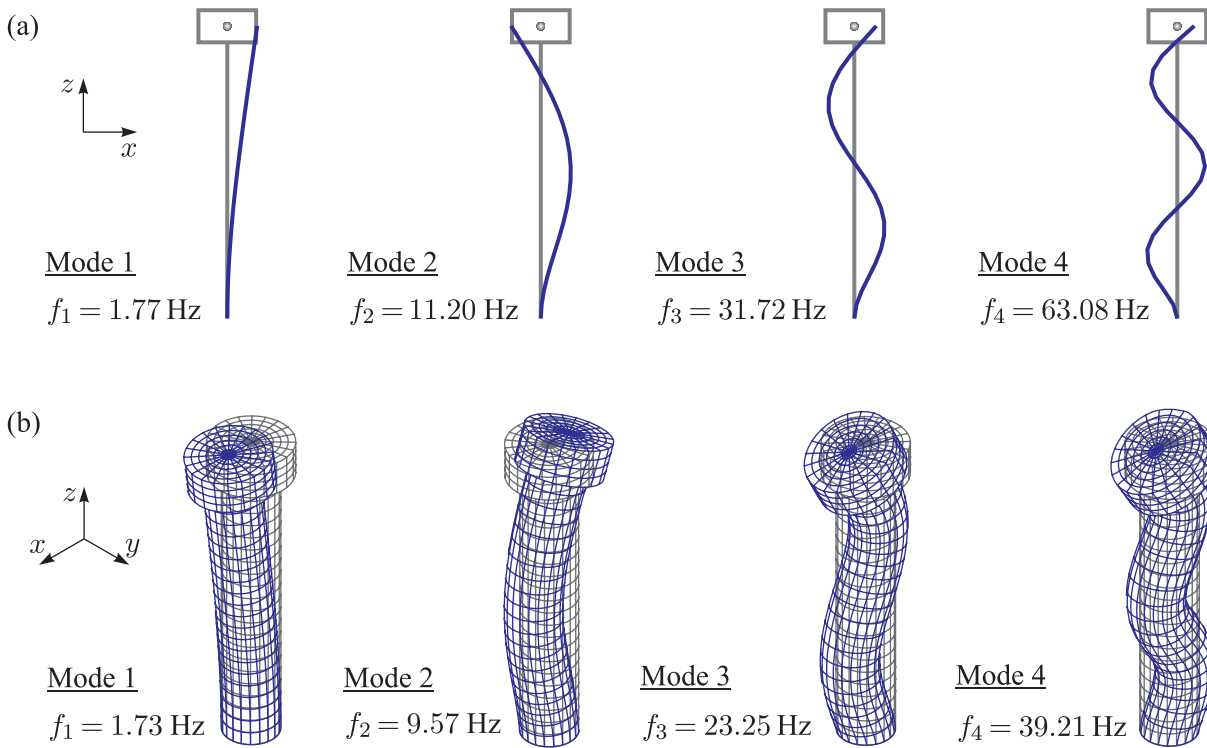


Figure 15. Mode shapes and corresponding frequencies of the axisymmetric tower studied in Example 2: (a) Analytical formulation; (b) Finite elements.

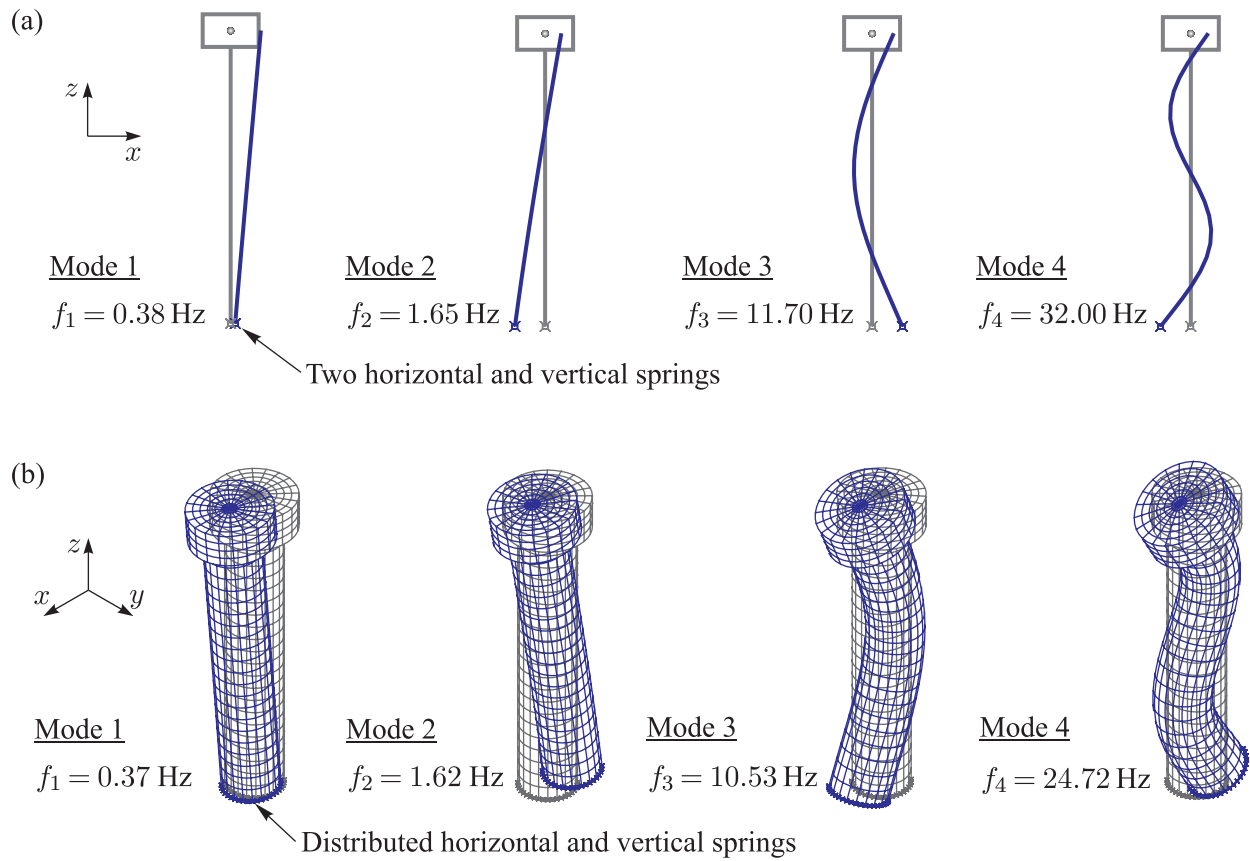


Figure 16. Mode shapes and corresponding frequencies of the axisymmetric tower studied in Example 2 including the effects of soil flexibility: (a) Analytical formulation; (b) Finite elements.

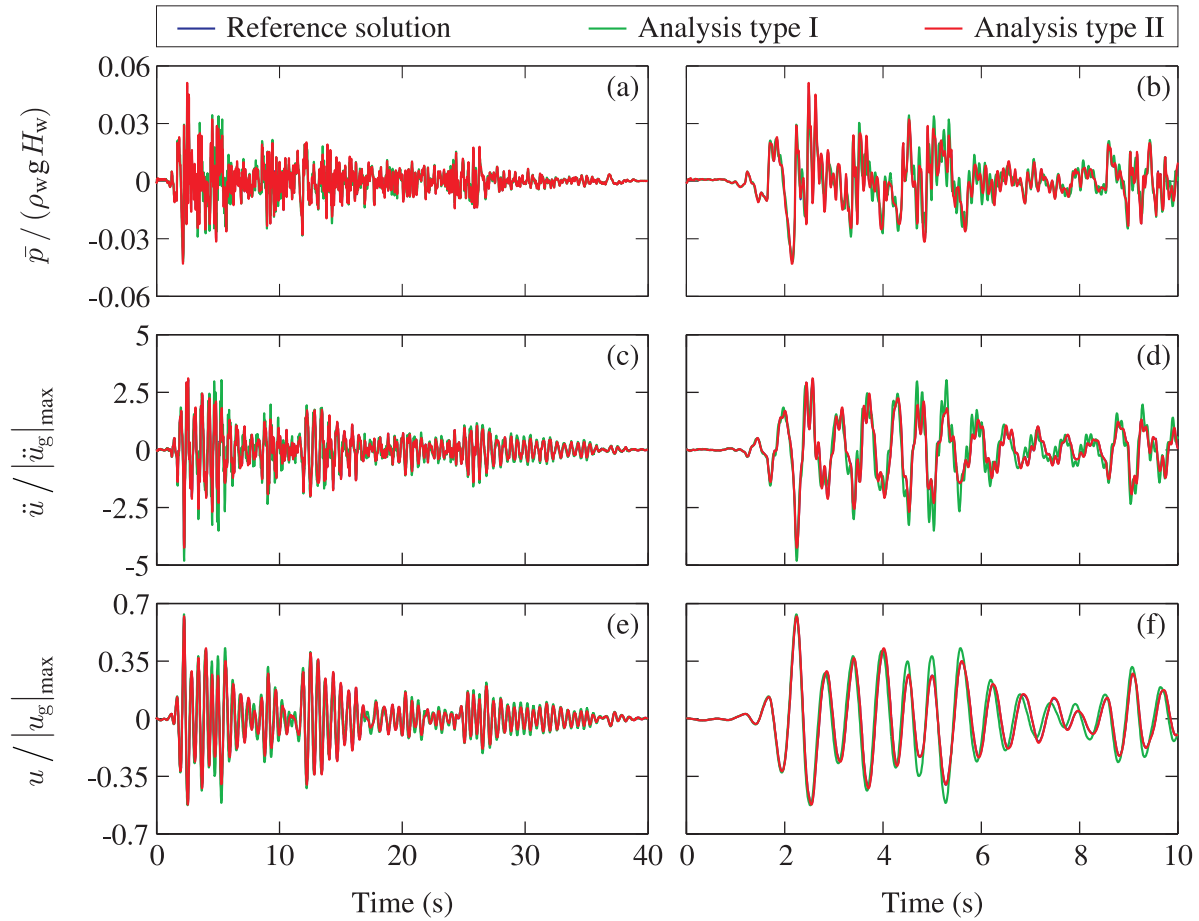


Figure 17. Time-histories of the seismic response of the axisymmetric tower studied in Example 2: (a) and (b) hydrodynamic pressure at point A; (c) and (d) horizontal acceleration at point B; (e) and (f) horizontal displacement at point B.

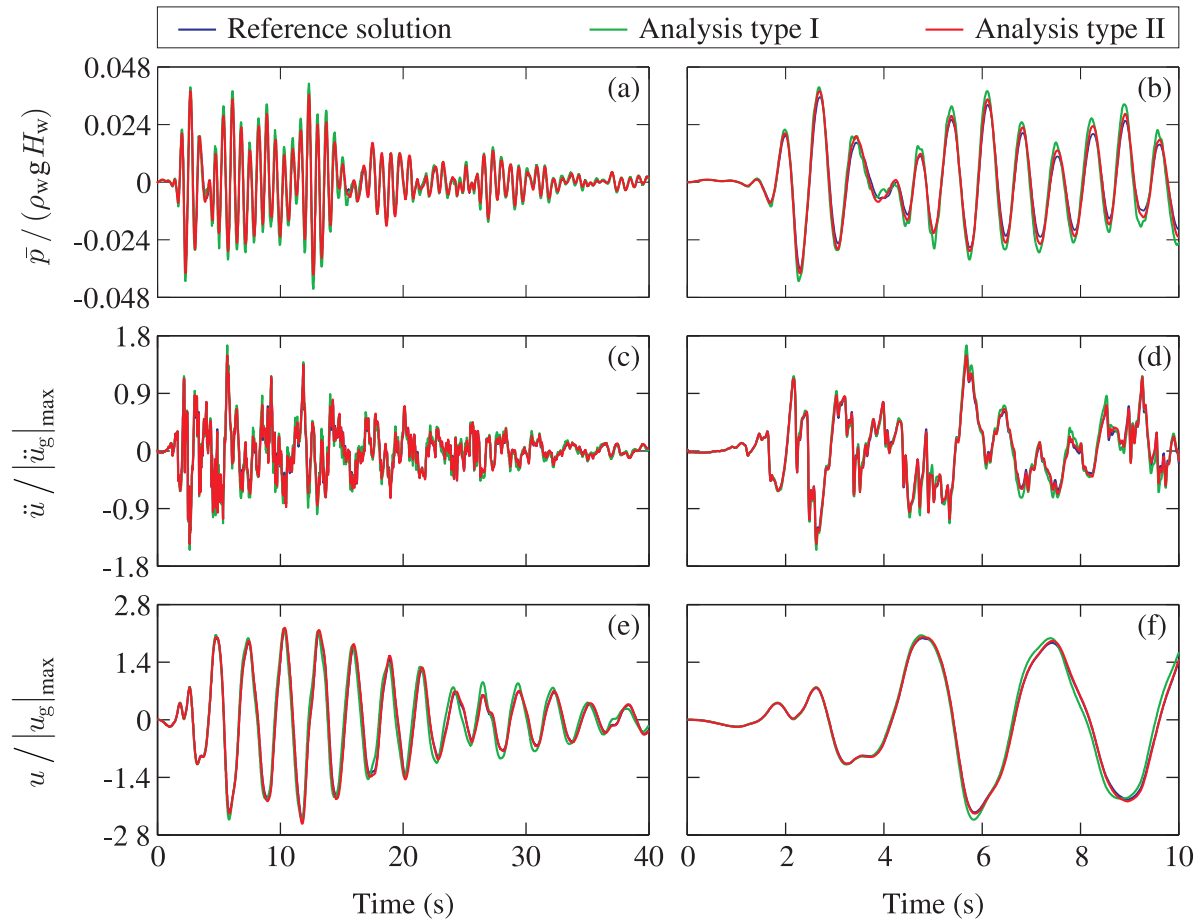


Figure 18. Time-histories of the seismic response of the axisymmetric tower studied in Example 2 including the effects of soil flexibility: (a) and (b) hydrodynamic pressure at point A; (c) and (d) horizontal acceleration at point B; (e) and (f) horizontal displacement at point B.

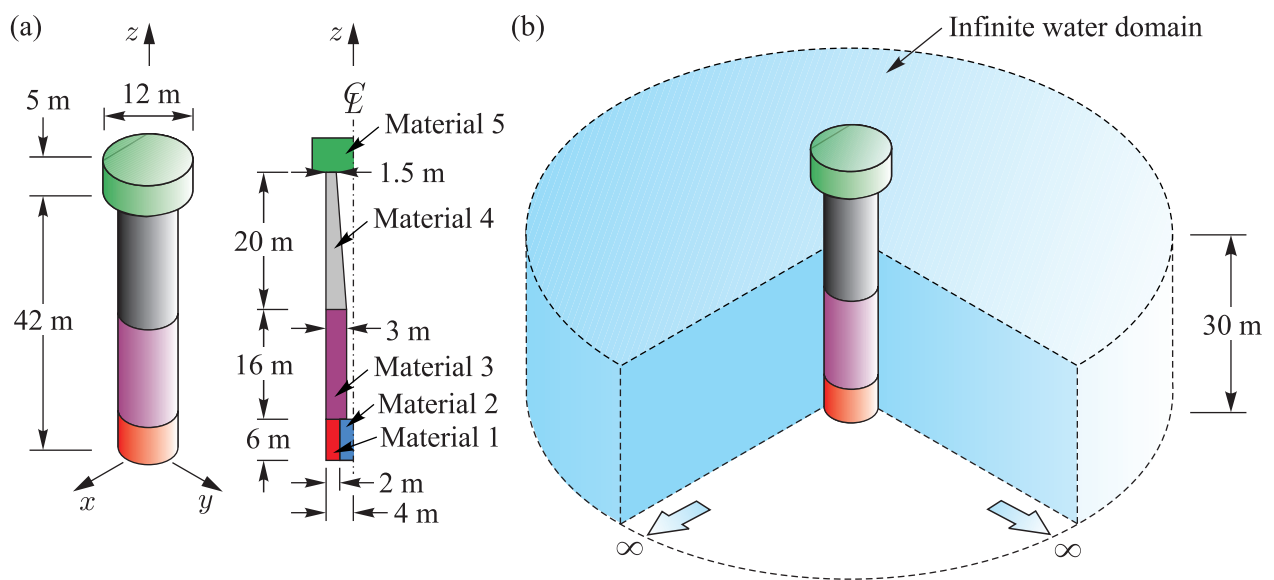


Figure 19. Axisymmetric tower studied in Example 3: (a) Geometry of the axisymmetric tower; (b) Tower surrounded by an infinite water domain.

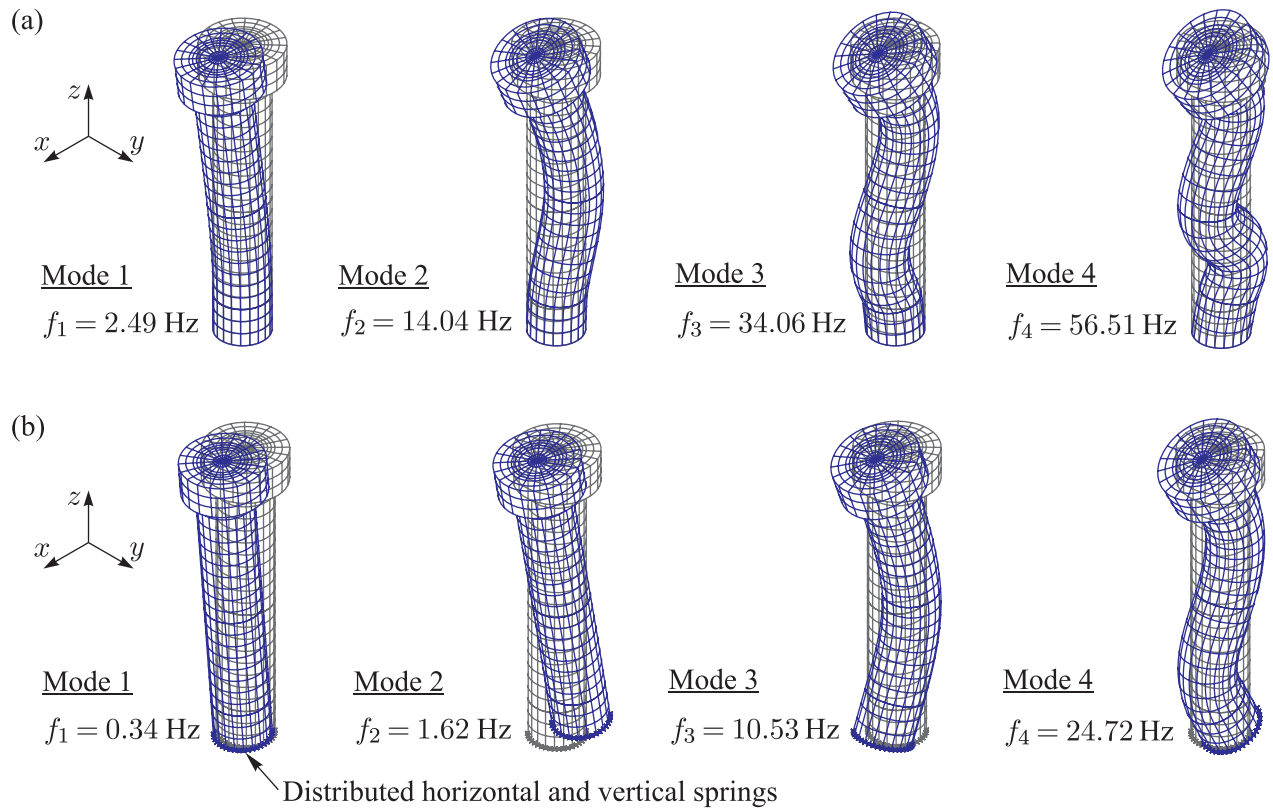


Figure 20. Finite element mode shapes and corresponding frequencies of the composite axisymmetric tower studied in Example 3: (a) Rigid soil; (b) Flexible soil.

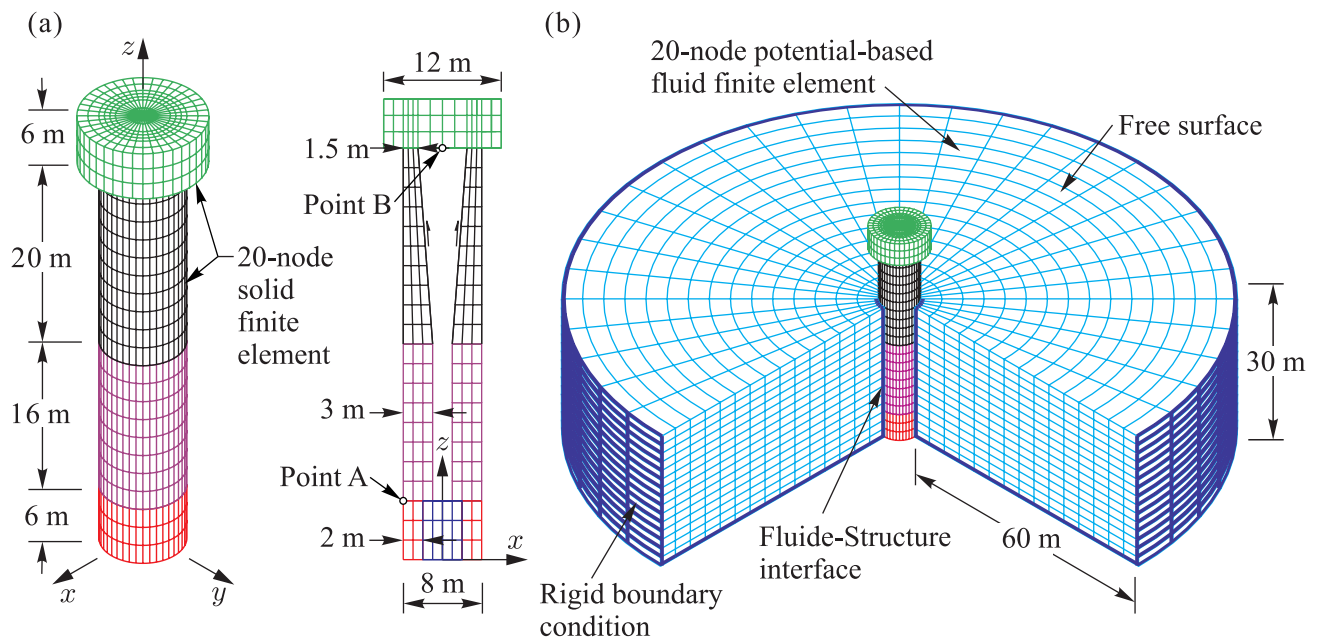


Figure 21. Finite element models of the composite axisymmetric tower studied in Example 3: (a) Finite element model of the structure without water; (b) Finite element model of the coupled tower-water system.

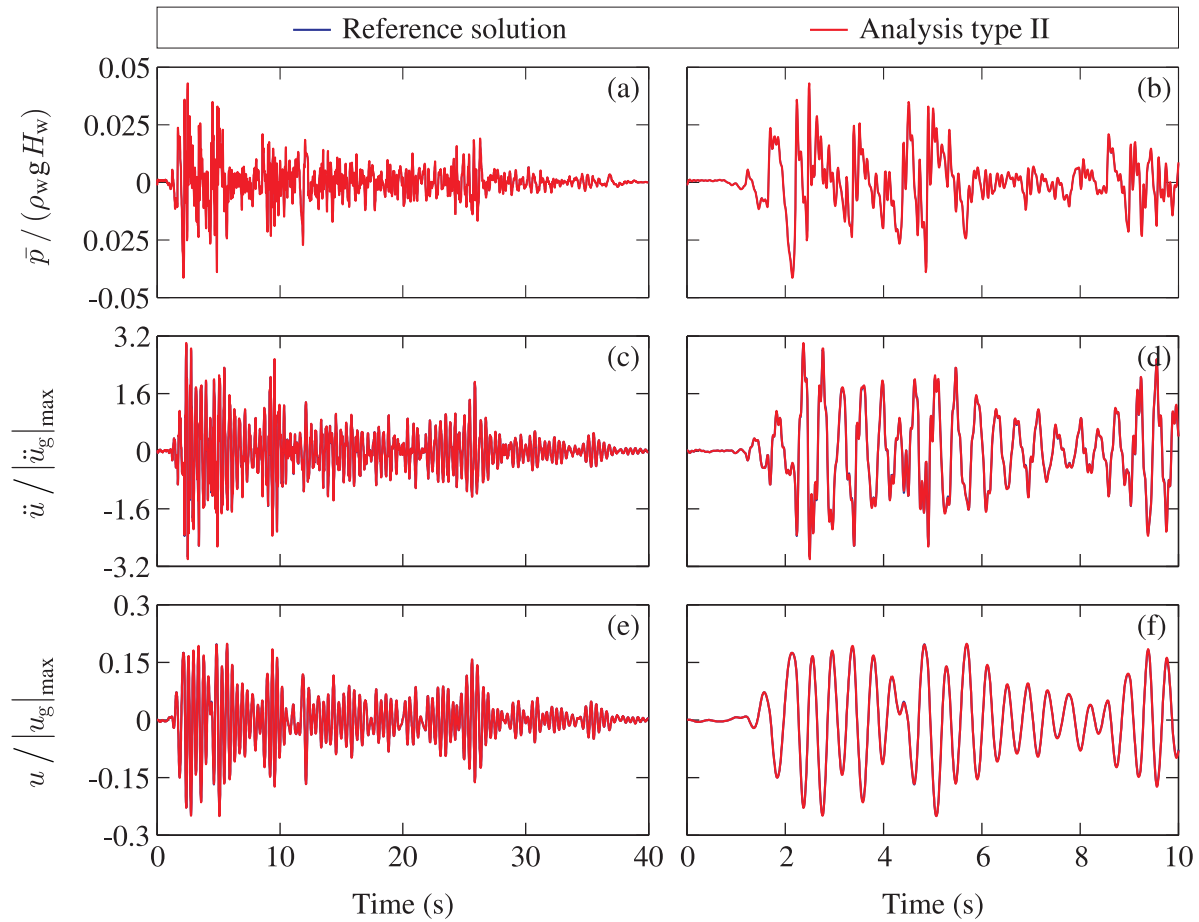


Figure 22. Time-histories of the seismic response of the composite axisymmetric tower studied in Example 3: (a) and (b) hydrodynamic pressure at point A; (c) and (d) horizontal acceleration at point B; (e) and (f) horizontal displacement at point B.

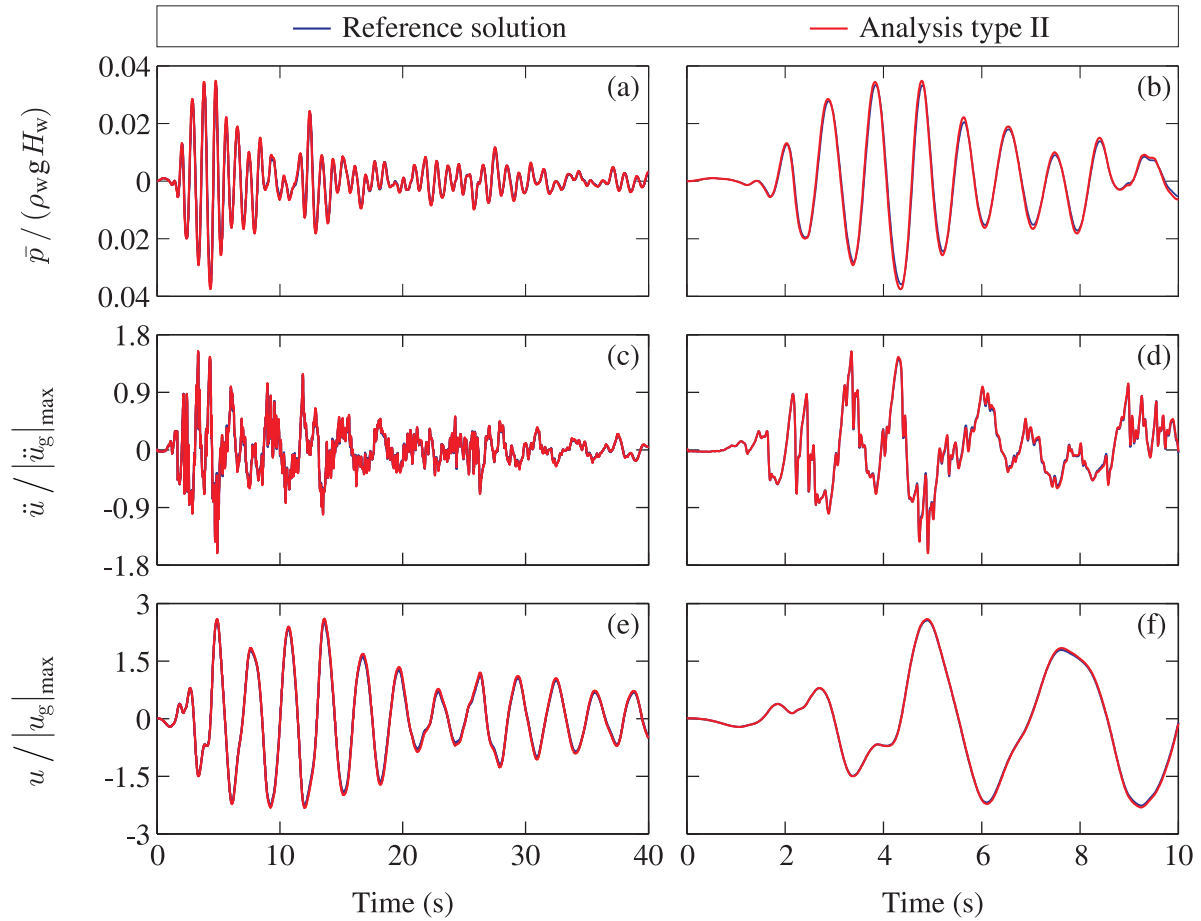


Figure 23. Time-histories of the seismic response of the composite axisymmetric tower studied in Example 3 including the effects of soil flexibility: (a) and (b) hydrodynamic pressure at point A; (c) and (d) horizontal acceleration at point B; (e) and (f) horizontal displacement at point B.

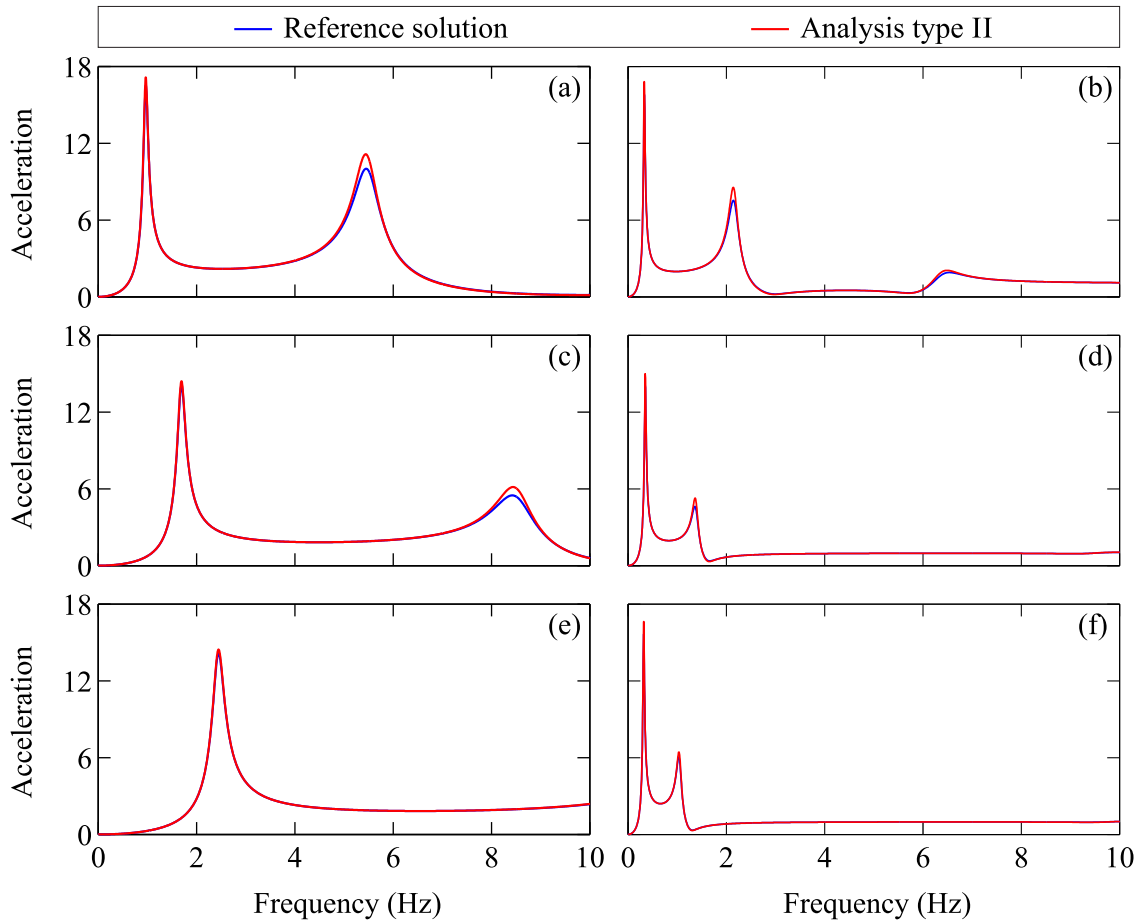


Figure 24. Frequency response functions for horizontal acceleration \bar{u} at point B of the tower-water systems studied: (a) Tower of Example 1 with rigid foundation; (b) Tower of Example 1 with flexible foundation; (c) Tower of Example 2 with rigid foundation; (d) Tower of Example 2 with flexible foundation; (e) Tower of Example 3 with rigid foundation; (f) Tower of Example 3 with flexible foundation.

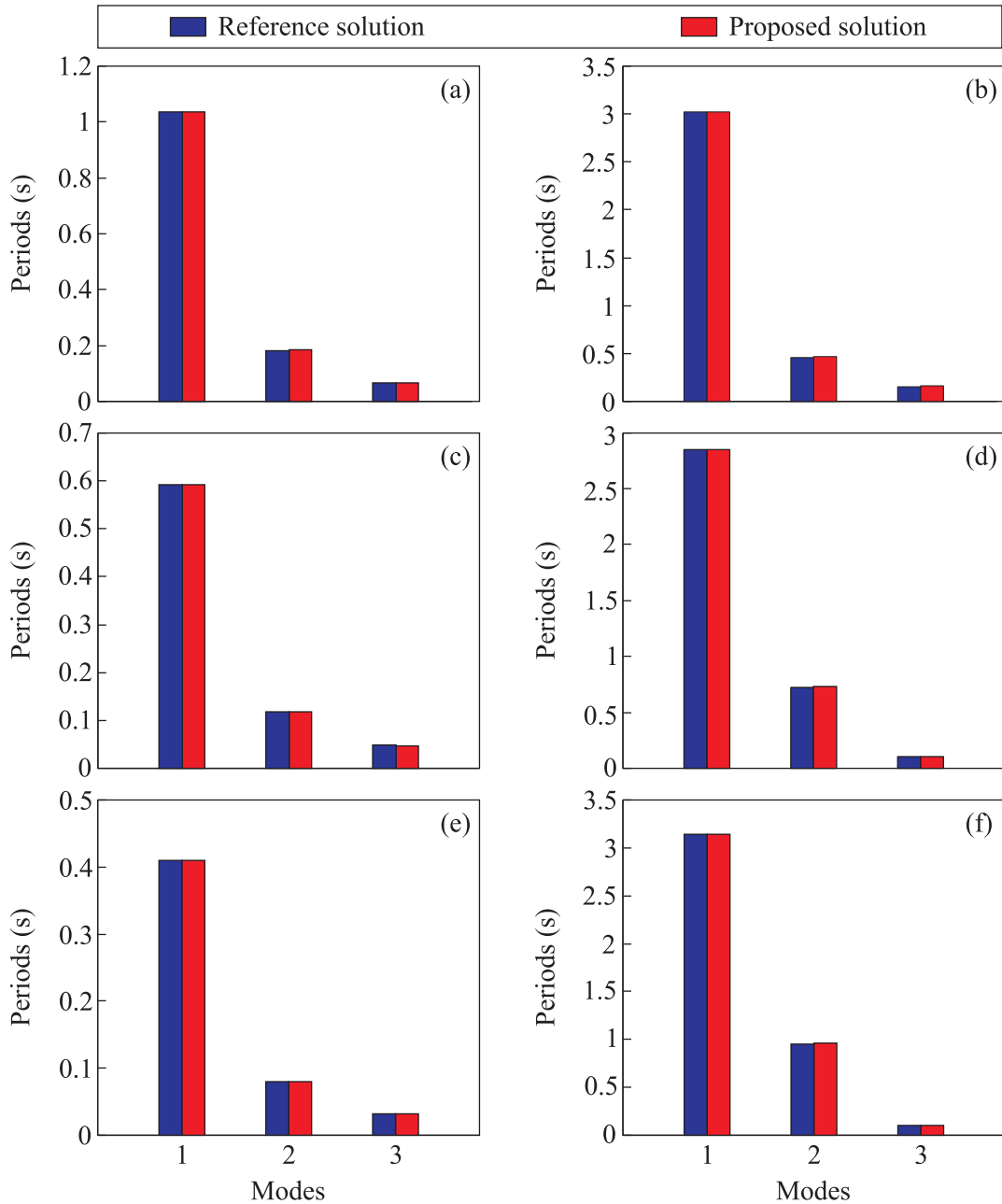


Figure 25. Vibration periods obtained using the reference and proposed solutions: (a) Tower of Example 1 with rigid foundation; (b) Tower of Example 1 with flexible foundation; (c) Tower of Example 2 with rigid foundation; (d) Tower of Example 2 with flexible foundation; (e) Tower of Example 3 with rigid foundation; (f) Tower of Example 3 with flexible foundation.

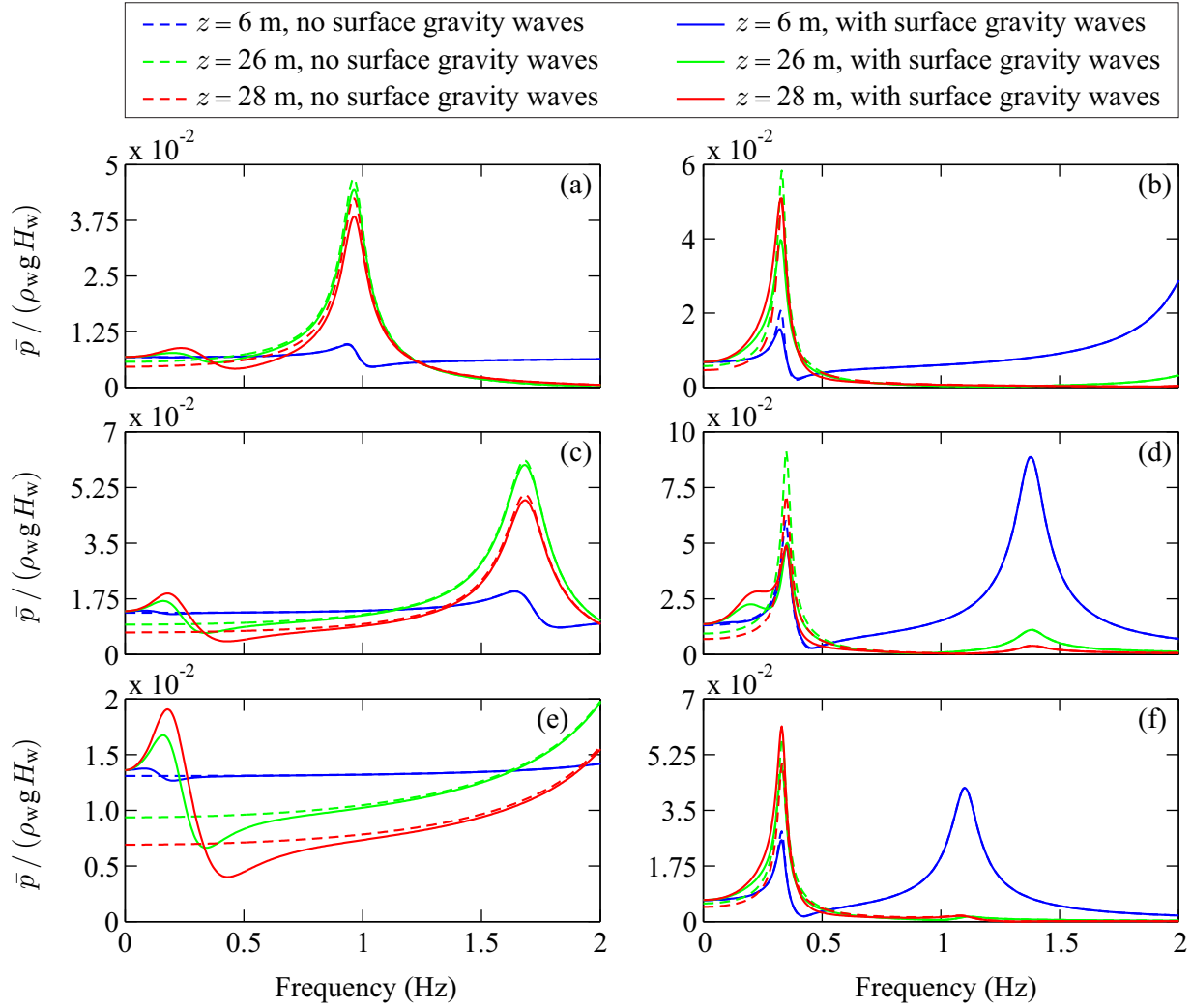


Figure 26. Nondimensionalized hydrodynamic pressure frequency response functions $\bar{p}/(\rho_w g H_w)$ obtained at three points of the structure-water interface, located at $z = 6$ m, $z = 26$ m and $z = 28$ m above the heel of each tower: (a) Tower of Example 1 with rigid foundation; (b) Tower of Example 1 with flexible foundation; (c) Tower of Example 2 with rigid foundation; (d) Tower of Example 2 with flexible foundation; (e) Tower of Example 3 with rigid foundation; (f) Tower of Example 3 with flexible foundation.

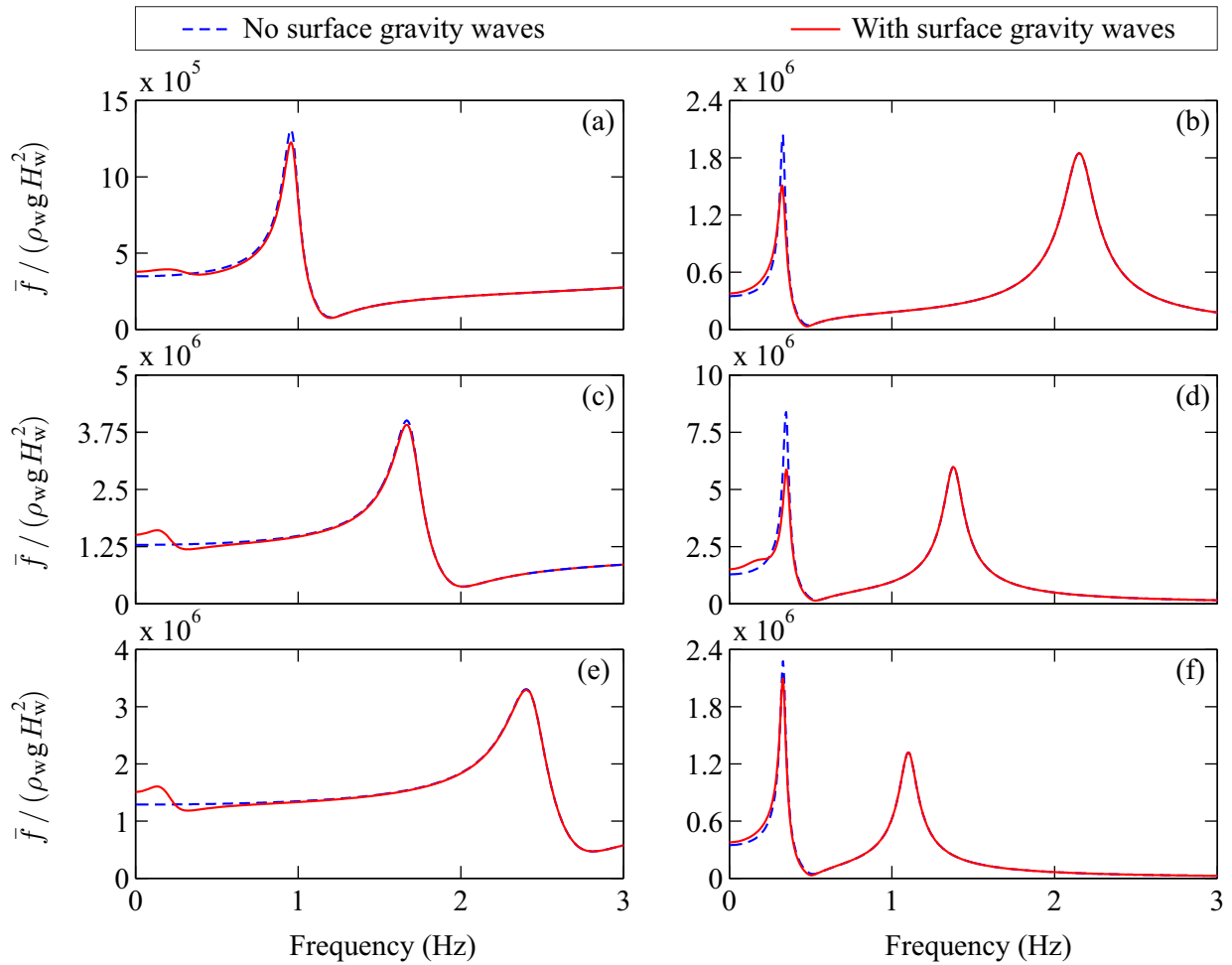


Figure 27. Nondimensionalized hydrodynamic force frequency response functions $\bar{f}/(\rho_w g H_w^2)$: (a) Tower of Example 1 with rigid foundation; (b) Tower of Example 1 with flexible foundation; (c) Tower of Example 2 with rigid foundation; (d) Tower of Example 2 with flexible foundation; (e) Tower of Example 3 with rigid foundation; (f) Tower of Example 3 with flexible foundation.

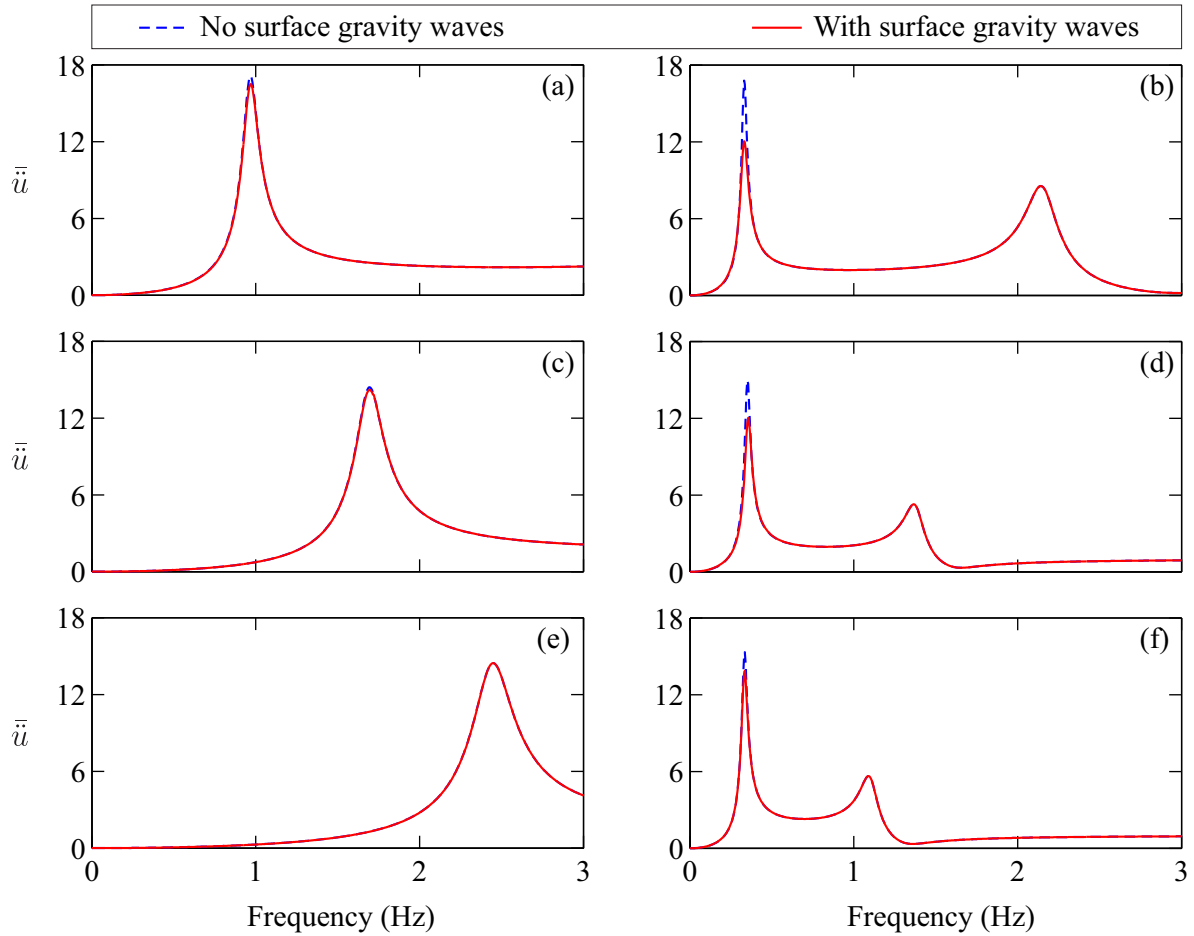


Figure 28. Frequency response functions for horizontal acceleration \ddot{u} at point B of the tower-water systems studied: (a) Tower of Example 1 with rigid foundation; (b) Tower of Example 1 with flexible foundation; (c) Tower of Example 2 with rigid foundation; (d) Tower of Example 2 with flexible foundation; (e) Tower of Example 3 with rigid foundation; (f) Tower of Example 3 with flexible foundation.